

## A Parameterization of Heterogeneous Land Surfaces for Atmospheric Numerical Models and Its Impact on Regional Meteorology

R. AVISSAR

*Department of Meteorology and Physical Oceanography, Cook College, Rutgers University, New Brunswick, New Jersey*

R. A. PIELKE

*Department of Atmospheric Science, Colorado State University, Fort Collins, Colorado*

(Manuscript received 25 July 1988, in final form 9 March 1989)

### ABSTRACT

Natural land surfaces are usually heterogeneous over the resolvable scales considered in atmospheric numerical models. Therefore, model surface parameterizations that assume surface homogeneity may fail to represent the surface forcing accurately.

In this paper, a parameterization of the subgrid-scale forcing of heterogeneous land surfaces for atmospheric numerical models is suggested. In each surface grid element of the numerical model similar homogeneous land patches located at different places within the element are regrouped into subgrid classes. Then, for each one of the subgrid classes, a sophisticated micrometeorological model of the soil-plant-atmosphere system is applied to assess the surface temperature, humidity, and fluxes to the atmosphere. The global fluxes of energy between the grid and the atmosphere are obtained by averaging according to the distribution of the subgrid classes. In addition to the surface forcing, detailed micrometeorological conditions of the patches are assessed for the domain simulated by the atmospheric model.

This parameterization was incorporated into a mesoscale numerical model to test the impact of subgrid-scale land surface heterogeneities on the development of local circulations. Where strong contrasts in total sensible heat flux are generated by land surface heterogeneities, circulations as strong as sea breezes may develop.

### 1. Introduction

It has been increasingly apparent in recent years that the distribution of surface sensible heat flux is a critical factor in producing and modifying the mesoscale atmospheric circulations often associated with terrain inhomogeneities such as land-sea boundaries, urban-rural areas, bare soil-vegetated areas, and mountain-valley structures (McNider and Pielke 1981; Garrett 1982; Zhang and Anthes 1982; Ookouchi et al. 1984; Sellers et al. 1986; Wilson et al. 1987; Segal et al. 1988). Therefore, the parameterization of the Bowen ratio ( $\beta$ ), i.e., the partition of energy between the sensible and the latent heat fluxes at the surface, is of prime importance in achieving accurate simulations with mesoscale atmospheric models. This ratio is strongly dependent on the availability of moisture at the surface; its value ranges from infinity in very dry regions to approximately zero over wet areas and may even be negative over vegetation under particular atmospheric conditions, e.g., the advection of dry air over a moist area (oasis effect). A variety of observational and

modeling evaluations of  $\beta$  have been reviewed by Segal et al. (1988).

Several representations of the land surface have been suggested for application in meteorological models. For instance, Pielke and Mahrer (1975) have computed the ground temperature through an energy budget equation for bare, dry soils. McCumber and Pielke (1981) introduced a refined parameterization of the soil layer and a bulk layer of vegetation following Deardorff (1978). Sellers et al. (1986) proposed a two-layer vegetation module to account for two different types of vegetation in a single grid element of their general circulation model. These parameterizations, however, all assume homogeneous land characteristics within a grid element.

In mesoscale meteorological models, however, one horizontal grid cell typically encloses a region of 10–100 km<sup>2</sup> and large inhomogeneities of soil type and soil wetness, of vegetation type and vegetation density, of topography, of urbanization, etc., are frequently present on this scale (Hills and Reynolds 1969; Wetzel and Chang 1988). Mahrer and Avissar (1985), for instance, demonstrated with a two-dimensional numerical soil model and field observations that temperature differences as large as 10°C occur between the north-facing and south-facing slopes of small furrows pro-

---

*Corresponding author address:* Dr. Roni Avissar, Department of Meteorology and Physical Oceanography, Cook College, Rutgers University, P.O. Box 231, New Brunswick, NJ 08903.

duced by agricultural tillage. In the same study, they also showed that while the south-facing slope of the furrows dried up quickly, the north-facing slope remained wet. Even larger gradients can be expected between the slopes of larger topographical features with the same inclination since no significant diffusion is possible between these slopes, in contrast to small furrows. Wetzel and Chang (1988) reported that for numerical weather prediction models with a grid spacing of 100 km or greater, the expected subgrid-scale variability of soil moisture may be as large as the total amount of potentially available water in the soil.

Because of such heterogeneities, the commonly used homogeneous surface parameterizations are inappropriate to represent the subgrid-scale spatial variability that is found in the real world, and, therefore, their use should be limited to rough evaluations and sensitivity analyses. In order to better represent the Bowen ratio and the fluxes associated with heterogeneous surfaces, one possibility is to increase the resolution of the model grid at the ground surface. Even though this method is probably the most accurate, it is usually not practical due to computer limitations and to the tremendous amount of data that would need to be gathered and processed in initializing the model. In addition, the applicability of the hydrostatic assumption used in many mesoscale numerical models is limited by the horizontal scale of the atmospheric forcing and response, and the grid size (Pielke 1984).

A more realistic solution to this problem was recently suggested by Avissar and Mahrer (1987). In order to improve the calculation of the diurnal variation in the actual evapotranspiration and the water balance of agricultural fields partially covered by vegetation and/or partially irrigated, they developed a pseudo-three-dimensional numerical model (Ps3D). In this model, the agricultural field is represented by patches of bare, dry soil and vegetated areas. Energy balance equations, surface energy fluxes, and soil moisture and temperature profiles are computed separately for each patch following a procedure described in detail by Avissar and Mahrer (1988a) which is based on Deardorff's (1978) bulk layer parameterization (hereafter referred to as BLP). Thus, Ps3D uses BLP for each homogeneous patch (the bare soil and the vegetated area) but is not identical to BLP which does not distinguish between the different patches and erroneously assumes that partially vegetated fields are homogeneous. In the Ps3D model, horizontal fluxes between the different patches are assumed to be small as compared to the vertical fluxes; the vertical fluxes from the patches or subgrid-scale areas are horizontally averaged to compute the global or total fluxes to the atmosphere from a grid cell. Simulating an agricultural field partially covered by vegetation with the Ps3D and BLP models, and comparing simulation results pointed out differences as large as 40% and  $350 \text{ W m}^{-2}$  for the daily field water balance and the sensible heat flux predictions,

respectively. As will be demonstrated in section 3, such a sensible heat flux can considerably modify the planetary boundary layer (PBL) characteristics. Also, large surface temperature and latent heat flux differences were computed by the two models. It is worthwhile mentioning that the computer resources required to run the Ps3D are not significantly higher than those for the BLP. This is because the resolution of the atmosphere remains unchanged and the agricultural field is represented by only two areas. The explicit representation of an orchard with a full three-dimensional model, on the other hand, would probably require the capacity of a supercomputer to account for each tree separately.

Adopting a similar approach, Wetzel and Chang (1988) developed a model to compute grid-cell-average evapotranspiration from four separate equations representing unstressed and water-stressed rates for both vegetation and bare soil, all of which can occur simultaneously within a grid element. Comparisons with estimated regional evapotranspiration from two extensive micrometeorological field programs supported their model under a wide range of conditions.

In the present study, a generalization of the Ps3D for the parameterization of subgrid-scale heterogeneous surface forcing is suggested (hereafter referred to as SSFP) and is incorporated into a mesoscale numerical model in order to evaluate its impact on land/atmosphere interactions. Predicted meteorological fields are compared, when possible, with results obtained with the same mesoscale model in which the BLP is used to represent the land surface. Various applications of this new parameterization are also emphasized.

## 2. The numerical model

The numerical model used in the present study consists of two modules, an atmospheric module and a land surface module, which interact by supplying boundary conditions to each other.

### a. The atmospheric module

The formulation of the atmospheric module is described comprehensively in Pielke (1974), Pielke and Mahrer (1975), Mahrer and Pielke (1977, 1978), and McNider and Pielke (1981). It will not be described again here for brevity. Studies conducted with this module have demonstrated its ability to realistically resolve mesoscale atmospheric fields (e.g., Pielke and Mahrer 1978; Segal et al. 1982; Abbs and Pielke 1986).

### b. The land surface module

#### 1) BULK LAYER PARAMETERIZATION

The parameterization of homogeneous surfaces, i.e., bulk layer parameterization (BLP) is described in detail in Avissar and Mahrer (1988a) and has been used by

Avissar et al. (1987) and Segal et al. (1988) to evaluate the impacts of vegetation on the generation and modification of mesoscale circulations. This scheme was validated against a field experiment (Avissar et al. 1986) and has proven its ability to accurately describe the microclimate of homogeneous agricultural fields under various environmental conditions and at different plant growing periods. Because of its fundamental contribution to the present study and the slight modifications brought about by the soil hydraulic properties, it will be described in detail here.

The surface is assumed to consist of two layers, a vegetation layer and a soil layer or, alternatively, a body of water.

(i) *Vegetation layer.* Assuming that the heat capacity of the vegetation is small as compared to the energy fluxes, the energy budget of this layer is written as

$$R_{Nv} + E_v + H_v = 0, \quad (1)$$

where  $R_{Nv}$ , the net radiation of the canopy, accounts for the contributions of the solar radiation ( $R_s$ ) and the thermal radiation from the atmosphere ( $R_L$ ) absorbed by the plant layer either directly or after being reflected from the soil surface. It also accounted for the thermal radiation emitted by the soil surface ( $\epsilon_G \sigma T_G^4$ ), the thermal radiation emitted by the vegetation ( $2\epsilon_v \sigma T_v^4$ ), and its reflected component from the soil surface. The net radiation is therefore defined as follows:

$$R_{Nv} = \sigma_f (1 - \alpha_v - t_v) \{1 + \alpha_G [1 - \sigma_f (1 - t_v)]\} R_s + \sigma_f \epsilon_v \{ [1 + (1 - \sigma_f)(1 - \epsilon_G)] R_L + \epsilon_G \sigma T_G^4 \} - \sigma_f \epsilon_v \sigma T_v^4 [2 - \epsilon_v \sigma_f (1 - \epsilon_G)]. \quad (2)$$

Here  $\alpha_v$ ,  $t_v$ ,  $\epsilon_v$ , and  $T_v$  are the albedo, transmissivity, emissivity, and temperature of the vegetation, respectively,  $\sigma$  is the Stefan-Boltzmann constant,  $\sigma_G$  and  $\epsilon_G$  are the albedo and emissivity of the soil surface, and  $\sigma_f$ , the shielding factor, represents the fractional coverage of the ground by the canopy. This factor is 1 for a completely covered surface and 0 for bare soil.

The latent heat flux between the vegetation and the surrounding air,  $E_v$ , is given as

$$E_v = \sigma_f \rho L_h u_* q_*, \quad (3)$$

where  $u_*$  and  $q_*$  are the friction velocity and the "flux humidity," respectively, calculated according to Businger et al. (1971),  $\rho$  is the air density, and  $L_h$  the latent heat of evaporation. The surface consists of one or more layers. When the soil is bare, the surface consists of one layer which is the soil surface. When vegetation is present, the surface consists of the soil surface and a number of vegetation layers equivalent to the leaf area index (LAI) of the vegetation. If, for instance, the leaf area index is 3, the surface has four layers: three of vegetation and the soil surface. Thus,  $\sigma_f$  expresses the relative contribution of the vegetation to

the total heat fluxes between the surface (composed of soil and vegetation) and the atmosphere. This parameter is defined by the expression

$$\sigma_f' = \frac{2LAI\sigma_f}{1 + 2LAI\sigma_f}, \quad (4)$$

where the factor 2 expresses that both sides of the leaves contribute to the heat fluxes. Several plant species have stomata only on one side of their leaves. In that case, this factor reduces to 1. Table 1 shows how  $\sigma_f'$  is influenced by the shielding factor and the leaf area index. For instance, for a vegetation that completely covers the soil surface ( $\sigma_f = 1$ ) and has a leaf area index of 3,  $\sigma_f'$  is 0.86 which means that the vegetation contributes to 86% of the total surface fluxes and, consequently, the soil surface contributes to 14% of these fluxes.

Using this formulation, the surface specific humidity,  $q(z_0)$ , required for the computation of  $q_*$ , is

$$q(z_0) = \sigma_f' q_{va} + (1 - \sigma_f') q_G = (2LAI\sigma_f q_{va} + q_G) / (1 + 2LAI\sigma_f), \quad (5)$$

where  $q_{va}$ , the specific humidity at the leaf-air interface, is computed following a procedure suggested by Avissar et al. (1985), i.e.,

$$q_{va} = d_{sr} q_v^* + (1 - d_{sr}) q_G, \quad (6)$$

where  $q_v^*$  is the saturated specific humidity at the leaf surface, and  $d_{sr}$  is the dimensionless relative stomatal conductance, defined as follows:

$$d_{sr} = [d_{sm} + (d_{sm} - d_{sm}) f_R f_T f_V f_C f_\Psi] / d_{sm}, \quad (7)$$

where  $d_{sm}$  is the minimal stomatal conductance which occurs only through the leaf cuticle when the stomata are closed,  $d_{sm}$  is the maximum stomatal conductance obtained when stomata are completely opened, and each of the  $f_i$  functions quantifies the influence of a specific environmental factor upon the conductance ( $R$  stands for solar global radiation,  $T$  for leaf temperature,  $V$  for vapor pressure difference between leaf and ambient air,  $C$  for ambient atmospheric carbon dioxide concentration, and  $\Psi$  for soil water potential in the

TABLE 1. Contribution of the vegetation to the total surface fluxes as a function of the shielding factor ( $\sigma_f$ ) and the leaf area index (LAI) of the vegetation.

$\sigma_f$	LAI		
	1	3	5
0	0	0	0
0.10	0.17	0.375	0.50
0.25	0.33	0.60	0.71
0.50	0.50	0.75	0.83
0.75	0.60	0.82	0.88
1.00	0.67	0.86	0.91

root zone). The expression used for each of these functions is

$$f_i = \frac{1}{1 + \exp[-S_i(X_i - X_{b_i})]}, \quad (8)$$

where the subscript  $i$  refers to the environmental factor,  $X_i$  is the intensity of the factor  $i$ ,  $X_{b_i}$  is the value of  $X_i$  at  $f_i = 1/2$ , and  $S_i$  is the slope of the curve at this point. If one of the environmental factors is in the critical range and should cause stomatal closure, then the value of its respective function is 0 and  $d_{sr} = d_{sm}/d_{sm}$ . When, however, the given environmental factor does not inhibit the stomatal opening, the value of its respective function is 1 and it does not influence  $d_{sr}$ . When all the  $f_i$  functions are equal to 1, i.e., when there is no environmental impact on the stomatal opening,  $d_{sr} = 1$  and the transpiration reaches its maximum value for the given meteorological conditions. The constants  $d_{sm}$ ,  $d_{sm}$ ,  $X_{b_i}$ , and  $S_i$  are empirically determined. For example, Avissar et al. (1985) provided their values for a tobacco plant. Further studies are still required to establish whether or not these constants are specific for each plant type and if they are constant within a single canopy.

The soil surface specific humidity,  $q_G$ , is computed following Avissar and Mahrer (1986):

$$q_G = s_w q_{Gu} + (1 - s_w) q(z_0). \quad (9)$$

Here  $q_{Gu}$  is the upper soil layer specific humidity calculated according to Philip and de Vries (1957),

$$q_{Gu} = q_{Gu}^* \exp(-g|\Psi_{Gu}|/R_v T_{Gu}), \quad (10)$$

with  $q_{Gu}^*$ ,  $\Psi_{Gu}$ , and  $T_{Gu}$  being the saturation specific humidity, the matric potential and the temperature of the upper soil layer. The gas constant of water vapor is  $R_v$  and  $g$  is the acceleration due to gravity.

The surface wetness function,  $s_w$ , is defined as follows:

$$s_w = a_w + \frac{1 - a_w}{1 + \exp[b_w(\eta_T - \eta)]}, \quad (11)$$

where  $\eta$  is the volumetric water content, and  $a_w$ ,  $b_w$ , and  $\eta_T$  are dimensionless empirical constants which depend upon soil type. For example, their value for Rehovot brown-red sandy soil (Xerorthant) were found to be 0.3, 32.0, and 0.06, respectively (Avissar and Mahrer 1986). This function is required to define the specific humidity at the soil-air interface (Eq. 9) which depends on the upper soil layer and the lower atmosphere specific humidities.

The sensible heat flux between the vegetation and the surrounding air,  $H_v$ , is

$$H_v = \sigma_f \rho c_p u_* \theta_*, \quad (12)$$

where  $c_p$  is the air specific heat at constant pressure. The value of  $\theta(z_0)$  needed for the calculation of the

“flux temperature”  $\theta_*$  [also calculated according to Businger et al. (1971)] is given by

$$\begin{aligned} \theta(z_0) &= \sigma_f' \theta_v + (1 - \sigma_f') \theta_G \\ &= (2LAI\sigma_f \theta_v + \theta_G) / (1 + 2LAI\sigma_f), \end{aligned} \quad (13)$$

with  $\theta_v$  and  $\theta_G$  being the potential temperatures of the vegetation layer and ground, respectively.

(ii) *Soil layer.* The energy budget of the soil surface, including both bare soil and covered soil, is given by the equation

$$R_{NG} + E_G + H_G + S_G = 0, \quad (14)$$

where  $R_{NG}$ , the net radiation at the soil surface, accounts for the solar radiation and the thermal radiation from the atmosphere directly absorbed by the soil surface, the solar radiation transmitted by the vegetation, part of the thermal radiation emitted by the vegetation, and the thermal radiation emitted by the soil surface. It also accounts for the reflection, by vegetation, of the thermal radiation emitted by the soil surface. It is therefore defined as follows:

$$\begin{aligned} R_{NG} &= (1 - \alpha_G)(1 - \sigma_f + \sigma_f t_v) R_s + (1 - \sigma_f) \epsilon_G R_L \\ &+ \sigma_f \epsilon_G \epsilon_v \sigma T_v^4 - \epsilon_G \sigma T_G^4 [1 - \epsilon_G \sigma_f (1 - \epsilon_v)]. \end{aligned} \quad (15)$$

The latent heat flux between the soil surface and the surrounding air,  $E_G$ , is

$$E_G = (1 - \sigma_f') \rho L_h u_* q_*, \quad (16)$$

and  $H_G$ , the sensible heat flux between the soil surface and the surrounding air, is

$$H_G = (1 - \sigma_f') \rho c_p u_* \theta_*. \quad (17)$$

The soil heat flux at the surface,  $S_G$ , is

$$S_G = -\lambda \left. \frac{\partial T_s}{\partial z} \right|_{z=0} = -\lambda \frac{T_G - T_{Gu}}{\Delta z}, \quad (18)$$

where  $T_s(z)$  is the subsurface soil temperature profile,  $T_{Gu}$  is the soil temperature at the depth  $z$ , and  $\lambda$  is the soil heat conductivity computed following a procedure suggested by de Vries (1963) which accounts for both the soil texture and the soil water content. The prediction of  $T_{Gu}$  is obtained by solving a finite difference representation of the soil heat diffusion equation,

$$C \frac{\partial T_s}{\partial t} = \frac{\partial}{\partial z} \left[ \lambda \frac{\partial T_s}{\partial z} \right]. \quad (19)$$

In order to realistically evaluate the soil thermal properties and the wetness of the upper soil layer (which is of primary importance for a correct evaluation of  $\beta$  at the soil surface) the soil moisture diffusion equation was also incorporated into the model, viz.

$$\frac{\partial \eta}{\partial t} = \frac{\partial}{\partial z} \left[ D_\eta \frac{\partial \eta}{\partial z} \right] + \frac{\partial}{\partial z} \left[ D_T \frac{\partial T_s}{\partial z} \right] + \frac{\partial K_h}{\partial z} - V_e, \quad (20)$$

where  $D_\eta$  and  $D_T$  are the isothermal and thermal moisture diffusivities, respectively [calculated according to Philip and de Vries (1957)]. The hydraulic conductivity,  $K_h$ , is obtained from an empirical power curve formula given by Clapp and Hornberger (1978),

$$K_h = K_{h_s} \left( \frac{\eta}{\eta_s} \right)^{2b+3}, \quad (21)$$

where  $\eta$  and  $\eta_s$  are the actual and saturation volumetric water contents, respectively, and  $K_{h_s}$  is the hydraulic conductivity at saturation. The constant  $b$  is specific to each soil type and must be determined empirically. The matric potential  $\Psi$  (needed to compute  $D_\eta$ ) is calculated from the power law

$$\Psi = \Psi_{cr} \left( \frac{\eta_s}{\eta} \right)^b, \quad (22)$$

where  $\Psi_{cr}$  is the matric potential at which the water content begins to be lower than the saturation water content in the  $\Psi(\eta)$  curve. This parameterization of the hydraulic properties was adopted here because values of  $\eta_s$ ,  $\Psi_{cr}$ ,  $K_{h_s}$ , and  $b$  are provided for the 11 U.S. Department of Agriculture soil textural classes.

The function  $V_e$  accounts for soil water extraction by roots due to plant transpiration and is proportional to the root distribution and the soil water potential (Avisar and Mahrer 1982).

The relative importance of the different coefficients in Eq. (20) was discussed by Philip and de Vries (1957) and tested in various field experiments (e.g., Avisar and Mahrer 1982, 1986).

Equations (1)–(18) are solved iteratively to find the four unknowns of the system ( $T_v$ ,  $T_G$ ,  $q_{va}$  and  $q_G$ , the vegetation and soil surface temperatures and humidities, respectively). Equations (19)–(22) are solved from the soil surface to the soil depth at which the water content is constant (due to the presence of water table) or at which  $\partial\eta/\partial z = 0$ .

(iii) *Body of water.* When a body of water (e.g., lake, pond, sea, or river) is present in the model domain, constant surface temperature and constant saturation humidity are assumed for the simulation. The roughness of water ( $z_0$ ) is calculated according to Clarke (1970) as

$$z_0 = 0.032u_*^2/g, \quad (23)$$

with the condition that  $z_0 \geq 0.15 \times 10^{-4}$  m.

## 2) SUBGRID-SCALE HETEROGENEOUS SURFACE FORCING PARAMETERIZATION

In order to represent heterogeneous land surfaces, each surface grid cell of the numerical model is divided into homogeneous subregions. The number of subregions depends on the number of different homogeneous patches that together constitute the grid cell. Assuming, as in the Ps3D, that horizontal fluxes between subgrid

areas are small as compared to the vertical fluxes and that the atmospheric conditions (e.g., radiation, air temperature, air humidity, and wind speed) remain constant across a grid element, patches of the same type located at different places in the grid can be regrouped into one subgrid surface class. If, for example,  $n$  small lakes each of  $A$  m<sup>2</sup> area are found in a single grid cell, then only one subgrid surface class "lake" of area  $nA$  m<sup>2</sup> will be defined for this grid cell. This aggregation procedure, of course, will generally reduce considerably the number of subgrid surface classes required per grid cell, as in this example. Then, for each one of the subgrid surface classes, the module described in section 2b(1) is applied. The global or total fluxes of energy from the surface to the atmosphere of each grid cell,  $\Phi_j^k$ , are evaluated in the SSFP according to the distribution of the different subgrid areas within the grid cell,

$$\Phi_j^k = \frac{\sum_{i=1}^n A_{i,j} \phi_{i,j}^k}{\sum_{i=1}^n A_{i,j}}, \quad (24)$$

where  $\phi_{i,j}^k$  is the particular flux considered from the subgrid surface class (the superscript  $k$  indicates the flux type—sensible heat flux, latent heat flux, longwave radiation, and so forth) and  $A_{i,j}$  is the total area of the subgrid surface class  $i$  from the  $n$  subgrid areas that compose the grid element  $j$ .

Note that when the BLP approach is used to represent a partially vegetated domain, the shielding factor  $\sigma_f$  may take on any value between 0 and 1, and the soil layer is assumed to be horizontally homogeneous regardless of the surface cover. With the SSFP, however, an arbitrary number of subgrid surface classes are permitted, so that the shielding factor  $\sigma_f$  may take on only one of two values; one in the case of a vegetation surface type and zero in the case of an unvegetated surface type such as bare soil or a water body. The soil layer beneath each surface class is independent of the soil layer beneath the other classes.

The microclimate close to the ground is strongly influenced by the surface properties and is, therefore, very different above a lake and above bare, dry soil under the same atmospheric conditions. With the bulk parameterizations of homogeneous surfaces there is no horizontal differentiation of the surface properties over a single grid cell and, therefore, only one "representative" value of the various fluxes is estimated. The parameterization described here computes the components of the microclimate for each different land patch. Therefore, in addition to a more realistic representation of the bottom boundary of the numerical models that should improve the quality of their simulations, a detailed description of the microclimate over the region considered by the atmospheric model is produced. It is worthwhile mentioning that this infor-

mation is of crucial importance for various applications in which the spatial distribution of micrometeorological data is used to infer the short-term energy or water budget of land surfaces, for instance, in agronomy, climatology, hydrology, and ecology. In remote sensing studies, a regional surface-energy budget that incorporates this parameterization may be inverted to infer evapotranspiration, and perhaps soil moisture, given satellite measurements of regional surface-emitted thermal radiation, and vegetation and soil properties.

The subgrid surface classes likely to appear in the subgrid-scale representation of heterogeneous land will be differentiated on the basis of soil type and wetness, vegetation type and density, and presence of urban areas, or bodies of water. These surface classes are characterized by their roughness, photometric properties, moisture availability, and heat capacity and conductance. Slopes with different inclinations and/or orientations receive different amounts of global solar radiation, resulting in variations of soil moisture and vegetation types and density. Such heterogeneities should also be represented by different subgrid classes. These subgrid surface classes were all defined for the present study, and a demonstration of how the SSFP scheme using these classes can affect regional meteorology is presented in section 3. Another land char-

TABLE 2. Soil properties and initial conditions.

Type	Density	Roughness
Clay-loam	1450 kg m <sup>-3</sup>	0.04 m
Hydraulic properties		
$\eta_s$	0.476	
$\Psi$	-0.63 m	
$K_{hs}$	0.216 m/day	
$b$	8.52	
Photometric properties		
$\alpha_G$	0.2	
$\epsilon_G$	0.95	
Number of soil levels		
13		
Initial profiles of temperature and wetness		
Soil depth (m)	Temperature (K)	Wetness (m <sup>3</sup> m <sup>-3</sup> )
0.00	300	0.04
0.01	300	0.04
0.02	300	0.04
0.03	300	0.04
0.04	300	0.04
0.05	300	0.25
0.075	300	0.25
0.125	300	0.25
0.20	300	0.25
0.30	300	0.25
0.50	300	0.25
0.75	300	0.25
1.00	300	0.25

TABLE 3. Vegetation input parameters.

Roughness	Leaf area index	Height
0.1 m	3	1.5 m
Photometric properties		
$\alpha_v$		0.15
$l_v$		0.125
$\epsilon_v$		0.98
Initial temperature		
300 K		
Root distribution with depth		
Soil depth (m)	Root percentage (%)	
0.00	00	
0.01	00	
0.02	00	
0.03	00	
0.04	00	
0.05	09	
0.075	12	
0.125	14	
0.20	18	
0.30	16	
0.50	16	
0.75	15	
1.00	00	

acteristic that may considerably modify the surface energy fluxes in snow cover. Because of the particular parameterization required for its representation, it was not incorporated in this study.

### 3. Model simulations

The model was run in its one- and two-dimensional versions in order to demonstrate the efficiency of SSFP in computing (i) the microclimate close to the ground in heterogeneous regions and, in particular, (ii) the resolved surface forcing for atmospheric numerical models. For the purpose of this study, the model was initialized with the parameters provided in Tables 2–5. The initial atmospheric vertical profiles of potential temperature ( $\theta$ ) and specific humidity ( $q$ ) reflect summer conditions in the subtropical regions. Segal et al. (1988) showed that in order to emphasize the impact of a partial cover of unstressed vegetation on mesoscale circulations using BLP, the soil must be initialized with a dry profile close to the surface and a wet profile in the root zone. This is because (i) a relatively high water content is necessary in the root zone to keep the plant stomata open (see Eqs. 7 and 8), and (ii) similar sensible heat fluxes are computed from a wet soil surface and an unstressed plant canopy [see Eqs. (9)–(11)]. Therefore, a wet soil surface reduces the influence of the partial cover of vegetation. In order to make possible a comparison between BLP and SSFP, the same initialization of the soil moisture profile was adopted for all the present simulations (Table 2). The soil tex-

TABLE 4. Atmospheric input parameters and initial conditions.

Number of vertical grid points	19
Number of horizontal grid points (2-D cases)	25
Horizontal grid increment	6 km
Synoptic flow	0.5 m s <sup>-1</sup> (unless otherwise specified)
Initial surface temperature	300 K
Initial potential temperature lapse	3.5 K/1000 m
Initial profile of specific humidity	
Height (m)	Humidity (g kg <sup>-1</sup> )
5	10.0
15	10.0
30	10.0
60	10.0
100	10.0
200	10.0
400	10.0
700	10.0
1 000	8.0
1 500	6.0
2 000	2.5
2 500	1.5
3 000	1.0
3 500	0.5
4 000	0.5
5 000	0.5
6 000	0.5
8 000	0.5
10 000	0.5

ture and hydraulic properties correspond to the "clay-loam" soil type of the U.S. Department of Agriculture soil textural classification (Clapp and Hornberger 1978).

a. Bare soil and vegetation

1) ONE-DIMENSIONAL SIMULATIONS

The diurnal variation of sensible heat flux, latent heat flux, and surface temperature for a bare soil ( $\sigma_f = 0$ ), and for the plant canopy and the soil surface of a completely covered soil ( $\sigma_f = 1$ ) are presented in Fig. 1. It should be remembered that for these two extreme situations, only one subgrid class is defined for SSFP and, therefore, SSFP and BLP produce identical results.

For these one-dimensional simulations, the atmosphere was homogeneously initialized with a geostrophic wind of 5 m s<sup>-1</sup>, resulting in a surface wind of  $2.8 \pm 0.6$  m s<sup>-1</sup> at a height of 5 m above the ground

TABLE 5. General model input parameters.

Integration time step	60 s
Latitude	37°N
Day of the year	July 15
Initialization time	0600 LST
Simulation time	12 hours

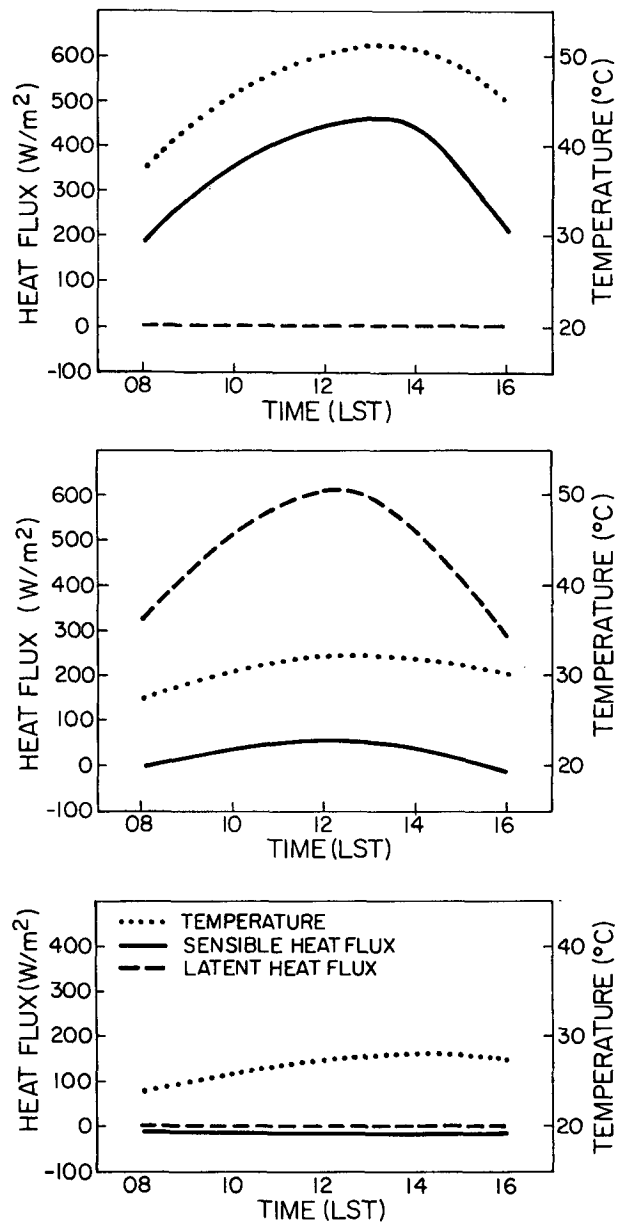


FIG. 1. The diurnal variation of sensible heat flux, latent heat flux, and surface temperature simulated with BLP and SSFP for a bare, dry surface ( $\sigma_f = 0$ ) and a dense unstressed vegetation which completely covers the soil surface ( $\sigma_f = 1$ ).

surface, depending on the hour of the day and the surface roughness.

For the bare soil (Fig. 1a), the sensible heat flux reaches a maximum during the afternoon of about 460 W m<sup>-2</sup>, the latent heat flux is zero all day long (due to the dry upper soil zone), and the soil surface temperature increases from 38°C at 0800 LST to 51°C at about 1300 LST. The Bowen ratio is, therefore, infinite. With  $\sigma_f = 1.0$  only about 10% of the solar-radiation penetrates through vegetation to the soil surface. As a result, the diurnal variation of the soil surface temper-

ature (Fig. 1c) is strongly damped as compared to the bare case, and a difference of temperature as large as 18°C is simulated between the bare and covered soil. The sensible heat flux from the soil varies between  $-5$  and  $-10 \text{ W m}^{-2}$ , indicating a transfer of energy from the atmosphere to the surface. Under the environmental conditions simulated in this case, the plant stomata remain open all day. Therefore, the energy absorbed by the vegetation is mainly converted to latent heat, leading to a maximum, at about noon, of  $610 \text{ W m}^{-2}$  (Fig. 1b). The sensible heat flux is about 10% of the latent heat flux ( $\beta \approx 0.1$ ). As reported by Segal et al. (1988) these results are in general agreement with observations.

The influence of the vegetation cover on the daily maximum sensible heat flux, latent heat flux, and surface temperature as produced by BLP and SSFP are presented in Fig. 2. The gradual increase of  $\sigma_f$  from 0.0 to 1.0 is not accompanied by a linear change of the global surface fluxes and temperatures. This is true especially with BLP for which the main changes occur between  $\sigma_f = 0.0$  and  $\sigma_f = 0.25$ . With this parameterization, the sensible heat flux drops from a maximum of  $460 \text{ W m}^{-2}$  for  $\sigma_f = 0.0$  to a maximum of  $150 \text{ W m}^{-2}$  for  $\sigma_f = 0.25$ ,  $90 \text{ W m}^{-2}$  for  $\sigma_f = 0.5$ ,  $75 \text{ W m}^{-2}$  for  $\sigma_f = 0.75$ , and  $70 \text{ W m}^{-2}$  for  $\sigma_f = 1.0$  (Fig. 2a). Corresponding values for the maximum latent heat flux (Fig. 2b) are 0, 300, 450, 560 and  $610 \text{ W m}^{-2}$ , and for the maximum surface temperature (Fig. 2c) are 51, 44, 38.5, 34, and  $32^\circ\text{C}$ .

With SSFP bare and vegetated areas are not combined together to produce one "representative" value for each of the fluxes and temperatures as with BLP, but different fluxes and temperatures are obtained for the bare and the vegetated areas, and global values are estimated according to Eq. (24). As a result, the dependency on  $\sigma_f$  is more linear and large discrepancies between the global values compared by BLP and SSFP are obtained, especially for the sensible heat flux.

The sensible heat flux and surface temperature of the soil surface simulated with BLP and SSFP as a function of the shielding factor, are represented in Fig. 3. As already emphasized, two separate sets of sensible heat flux and temperature are obtained with SSFP for  $0 < \sigma_f < 1$  (one for the bare part of the domain and one for the covered part), and only one set is obtained with BLP. Of course, for  $\sigma_f = 0$  there is no covered soil and for  $\sigma_f = 1$  there is no bare soil with SSFP, and, therefore, values are "missing" in this figure. The latent heat flux and the temperature of the canopy simulated with the two parameterizations are given in Fig. 4.

It is interesting to note that the surface temperature computed with BLP for  $\sigma_f = 0.25$  is  $1.5^\circ\text{C}$  higher than for the bare soil (Fig. 3b). This unexpected result is mainly due to the fact that the sensible heat flux (Fig. 3a) is reduced more than the latent heat flux from the vegetation (Fig. 4a) is increased ( $310 \text{ W m}^{-2}$  vs  $300 \text{ W m}^{-2}$ ). Even though there is no evaporation from

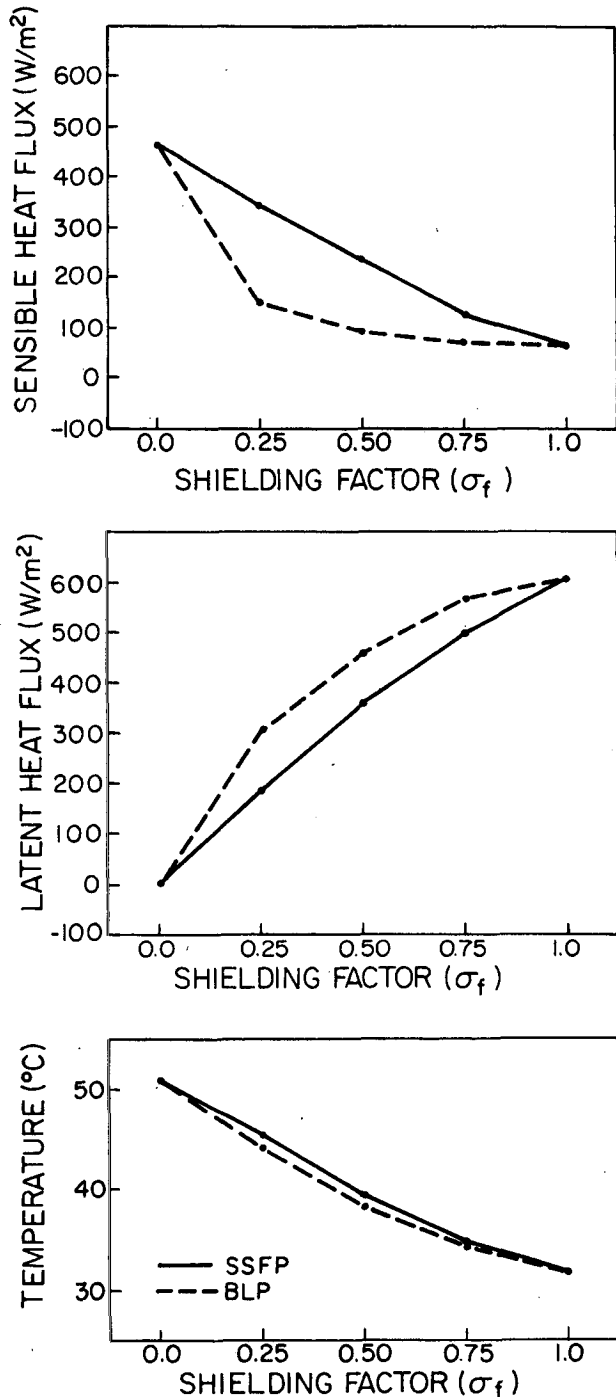


FIG. 2. The influence of the shielding factor on the daily maximum global sensible heat flux, latent heat flux, and surface temperature simulated with BLP and SSFP.

the soil surface, the combination of the vegetation and the soil fluxes in this type of parameterization, erroneously assuming homogeneity of the surface and of the soil layer, leads to such shortcomings. With SSFP, the sensible heat fluxes from the bare soil and the veg-

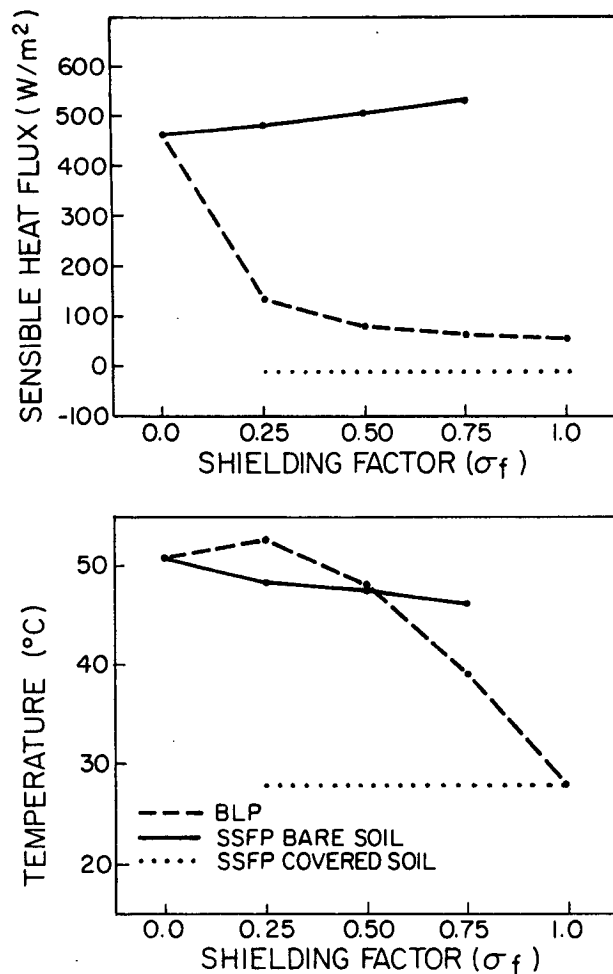


FIG. 3. The influence of the shielding factor on the daily maximum sensible heat flux from the soil surface and the surface temperature simulated with BLP and SSFP.

etation slightly increase with  $\sigma_f$ . Since, however, the sensible heat flux from the vegetation is very small (not represented here), and most of the time, it is even negative, the more the soil is covered by vegetation, the smaller the global sensible heat flux from the surface. For  $\sigma_f = 0.25$ , the predicted global sensible heat flux is  $330 \text{ W m}^{-2}$  (Fig. 2a). Respective values for  $\sigma_f = 0.5$  and  $\sigma_f = 0.75$  are 230 and  $120 \text{ W m}^{-2}$ . With the reduction of the global sensible heat flux to the atmosphere, the heating and the reference air temperature above the surface decrease. Since the energy absorbed per unit area by the bare soil and the vegetation patches remains essentially unchanged, the vertical gradient of temperature between the different patches and the atmosphere increases, also increasing their sensible heat flux. In contrast, the global latent heat flux to the atmosphere increases with the augmentation of the vegetation cover, and, consequently, the vertical gradient of specific humidity between the vegetation patch and

the atmosphere decreases. As a result, the latent heat flux from the vegetation (Fig. 4a) decreases too. For  $\sigma_f = 0.25, 0.5, 0.75$ , and  $1.0$ , latent heat fluxes of  $785, 720, 660$ , and  $610 \text{ W m}^{-2}$  are computed, respectively.

The discrepancies between the two parameterizations are very large for  $\sigma_f = 0.25$  and tend to diminish with the augmentation of the vegetation cover. From a micrometeorological point of view (which may be crucial for agricultural, ecological, and other applications) differences of sensible heat flux, latent heat flux, and soil surface temperature between the bare soil area or the vegetated area predicted with SSFP and the "representative" values predicted with BLP are as large as  $450 \text{ W m}^{-2}$  (for  $\sigma_f = 0.75$ ),  $440 \text{ W m}^{-2}$  (for  $\sigma_f = 0.25$ ), and  $19^\circ\text{C}$ , respectively. From an atmospheric modeling point of view, knowledge of the global forcing from the surface is more important than knowledge of the detailed micrometeorology. As already discussed, the sensible heat flux is particularly pertinent for this type of modeling. The differences between the global sensible heat flux obtained with SSFP and with BLP were  $190, 150$ , and  $50 \text{ W m}^{-2}$  for  $\sigma_f = 0.25, 0.50$ , and  $0.75$ , respectively (Fig. 2). The two-dimensional ver-

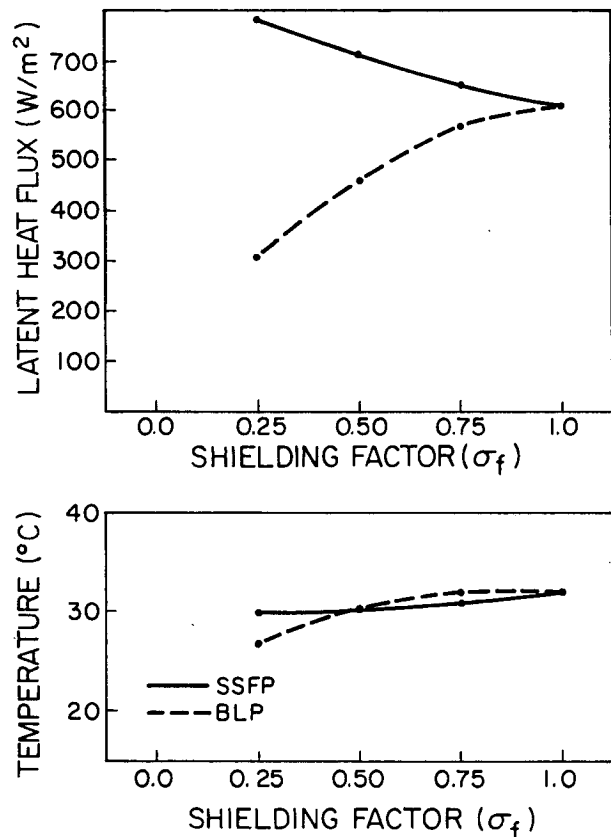


FIG. 4. The influence of the shielding factor on the daily maximum latent heat flux from the vegetation and the plants' temperature simulated with BLP and SSFP.

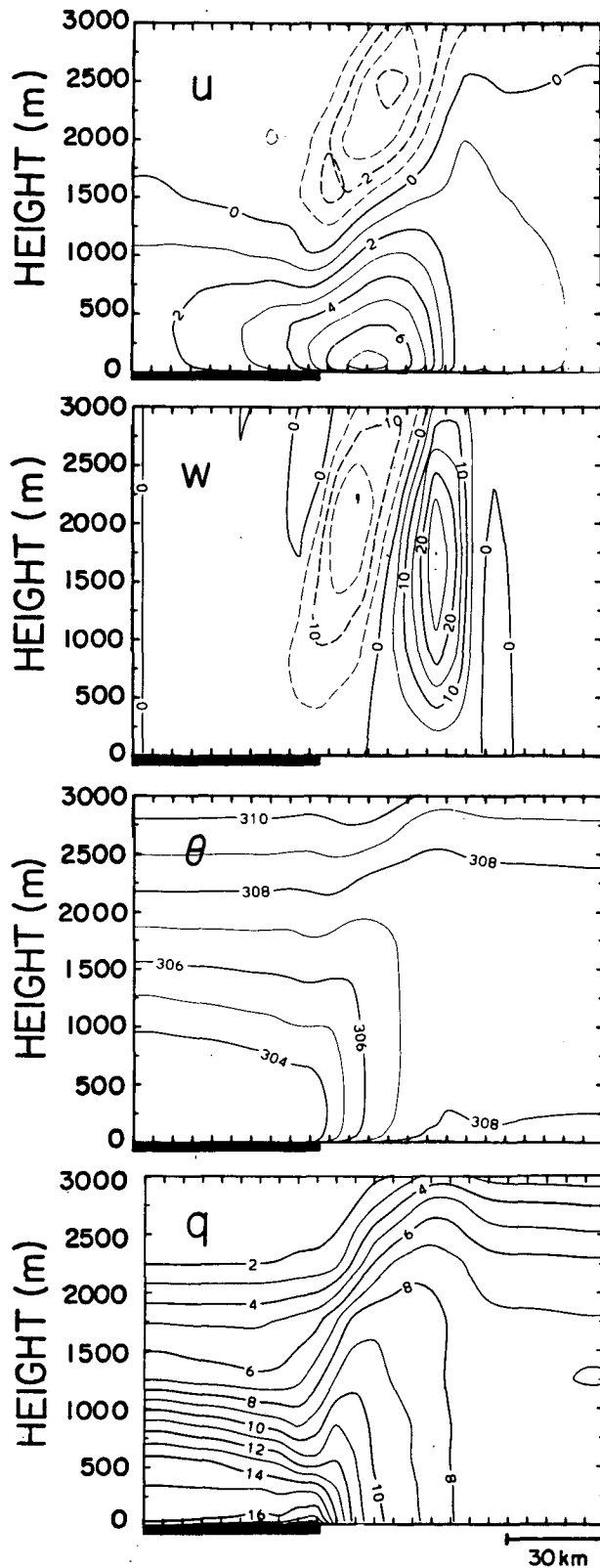


FIG. 5. Vertical cross section of the simulated domain at 1400 LST for (i) the horizontal wind component parallel to the domain ( $u$ ) in  $\text{m s}^{-1}$ , positive from left to right; (ii) the vertical wind com-

ponent ( $w$ ) in  $\text{cm s}^{-1}$ , positive upward; (iii) the potential temperature ( $\theta$ ) in K; and, (iv) the specific humidity ( $q$ ) in  $\text{g kg}^{-1}$ , resulting from the contrast of 60 km of dense unstressed vegetation (indicated by the dark underbar) and 90 km of bare, dry land. The vegetation completely covers the left-hand soil surface. Solid contours indicate positive values; dashed contours indicate negative values.

## 2) TWO-DIMENSIONAL SIMULATIONS

A study of vegetation effects on the generation and modification of mesoscale circulations was recently presented by Segal et al. (1988). They suggested that extensive unstressed vegetated areas may significantly reduce the strength of sea breezes and thermally induced upslope flows and, when juxtaposed with bare, dry land, such vegetated areas may generate local circulations as strong as sea breezes. Figure 5 illustrates such a circulation produced by juxtaposing a 60-km-wide strip of unstressed dense vegetation ( $\sigma_f = 1.0$ , LAI = 3) with a 90-km-wide strip of bare, dry soil. The entire domain is represented in the numerical model by 25 grid increments of 6 km width. This simulation was also designed to provide a control case to which other simulations may be compared. Since the vegetated domain is completely covered by vegetation, both BLP and SSFP are applicable for this type of simulation and give identical results. The model integration commenced at 0600 LST, which corresponds to the time when sensible heat fluxes typically become effective in the development of the convective PBL on sunny summer days. The meteorological fields shown in Fig. 5 ( $u$  is the horizontal component of the wind parallel to the domain,  $w$  is the vertical component of the wind,  $\theta$  is the potential temperature, and  $q$  is the specific humidity) are values at 1400 LST. By that hour, the circulation is strongly developed, as indicated by the intensity of  $u$  and  $w$  and by the thermal contrast shown by the  $\theta$  field. The component of the wind perpendicular to the domain is about  $0.15u$  at this hour, and thus is not of significance for purposes of illustration. Only later in the day does its intensity increase significantly as a result of the Coriolis effect. A shallow PBL develops over the vegetated area as can be seen from the  $\theta$  field. Transpiration over the vegetation provides a supply of moisture that significantly increases the amount of water vapor present in the shallow PBL. This moisture is advected by the thermally induced flow toward the dry region where it is well mixed within the relatively deep convective PBL. A similar simulation executed by Segal et al. (1988), but with a horizontal grid resolution of 3 km, gave approximately identical results, except for  $w$  for which the peak value was about two times stronger than the  $30 \text{ cm s}^{-1}$  computed in the present case. This well known dependency of  $w$  upon grid resolution

in numerical models is related to the solution of the continuity equation (e.g., Pielke 1984).

The magnitude of the local circulation can be estimated from the horizontal gradient of sensible heat flux. Pielke (1984), in reporting the results of observational and numerical studies (e.g., Hanna and Gifford 1975; Hanna and Swisher 1971), explained that it has been found that, in the tropics and midlatitudes, a horizontal gradient of less than about  $10 \text{ W m}^{-2}$  per 30 km has only a minor influence on local wind patterns. With a gradient of  $100 \text{ W m}^{-2}$  per 30 km, however, significant effects are discernible from the statistical evaluation of observational data, whereas a gradient of  $1000 \text{ W m}^{-2}$  per 30 km has been found to have a pronounced influence on local wind patterns in case-by-case studies. With reference to the results presented in section 3a(1), partial rather than complete vegetation cover would be expected to generate weaker circulations. Also, due to the difference of sensible heat flux evaluated with BLP and SSFP, different circulation intensities would be expected to result from the two parameterizations.

Figure 6 presents the meteorological fields at 1400 LST computed with BLP and SSFP by juxtaposing a 60-km-wide strip of unstressed vegetation which covers only one-fourth of the domain with a 90-km-wide strip of bare, dry soil. The simulation executed with SSFP exhibit significant differences as compared to that made with BLP. For instance, the peak intensities of  $u$  and  $w$  are about half those obtained with BLP ( $3.1 \text{ m s}^{-1}$  vs  $5.9 \text{ m s}^{-1}$  and  $13 \text{ cm s}^{-1}$  vs  $24 \text{ cm s}^{-1}$ , respectively). The reason for these differences is due to the apparently too large reduction of sensible heat flux by vegetation in BLP, as illustrated in Fig. 2a and Table 1 by the value of the coefficient  $\sigma'_f$  (Eq. 4) as a function of the vegetation cover. For  $\sigma_f = 0.25$  and  $\text{LAI} = 3$  (which were assumed in the simulations), for instance,  $\sigma'_f$  is 0.6, which means that the vegetation contributes to 60% of the total surface fluxes over the lefthand side of the domain. For higher values of  $\sigma_f$ , however, this coefficient offers a more realistic value. It is worth noting that as  $\sigma_f$  decreases the efficiency of transpiration from the canopy increases (although the total latent heat flux averaged over the grid area decreases). Physically, as the canopy coverage is reduced, the sensible heat flux released from the bare soil surface within the grid cell is advected to the canopy and is used to enhance transpiration which may then be larger than the available net radiation (e.g., Shaw and Decker 1977).

Similar simulations to those depicted in Fig. 6 were executed for vegetation which covers one-half and three-fourths of the 60-km-wide strip juxtaposed with a 90-km-wide strip of bare, dry soil. The strong non-linearity depicted for the fluxes and temperatures computed with BLP due to increasing the vegetation cover was again observed here. For  $\sigma_f = 0.25, 0.50, 0.75$  and  $1.0$ , the peak intensity of  $u$  was about  $5.9, 6.4, 6.6$  and  $7.2 \text{ m s}^{-1}$ , respectively, and the peak intensity of  $w$  was

about  $24, 27, 29$  and  $30 \text{ cm s}^{-1}$ , respectively. With SSFP, the peak intensity of  $u$  was about  $3.1, 5.1, 6.5$  and  $7.2 \text{ m s}^{-1}$ , respectively, and the peak intensity of  $w$  was about  $13, 19, 25,$  and  $30 \text{ cm s}^{-1}$ , respectively. A comparison between the potential temperature fields showed that the temperature profile and the height of the PBL above the bare part of the domain were not affected by the value of  $\sigma_f$ . In the vegetated part of the domain, however, the larger the vegetation cover, the smaller the global sensible heat flux and, consequently, the lower the temperature and the lower the height of the PBL.

The numerical experiments reported here were incorporated in the present study in order to demonstrate not only the shortcomings, but also the relative reliability of using a parameterization of the surface that assumes homogeneous land to describe a simple case of surface heterogeneity. From these simulations it can be inferred that the microclimate close to the ground surface is very poorly represented with the BLP. This is related to the totally different distribution of energy over a bare, dry soil and a transpiring vegetation layer. A "representative" value of the micrometeorological conditions, which is a kind of average value, is therefore far from either of the extreme conditions. From an atmospheric point of view, however, the detailed fluxes from the different surface classes combine together to generate a global forcing. Therefore, a simple parameterization for the evaluation of the "representative" surface forcing conditions may be appropriate for simple heterogeneous regions. The more heterogeneous the land surface, however, the less applicable the "representative" assumption. In the next two sections, land with more complex heterogeneities that cannot be represented with BLP are simulated with SSFP.

### b. Hilly regions

Extensive flat homogeneous regions are rarely found in the real world. Usually, even when the main topographical feature of a region can be assumed horizontal, the earth's surface consists of numerous small hills and valleys of different slope and orientation. Although these small variations of the topography may not be of direct significance for atmospheric processes, the orientation of the terrain with respect to the sun is a critical parameter for the evaluation of the amount of solar radiation received at the soil surface (Fig. 7). In addition, Sharon (1980) has observed that the amount of rain received at the ground surface is also strongly related to the orientation of the terrain. For these reasons, the availability of water for natural plants and the microclimate near the land surface may vary considerably with the surface's orientation. It is, therefore, not uncommon in semi-arid and arid regions to observe a bare, dry south-facing slope adjacent to a north-facing slope covered with dense vegetation. Figure 8 is an example of such strong contrast; the photograph was

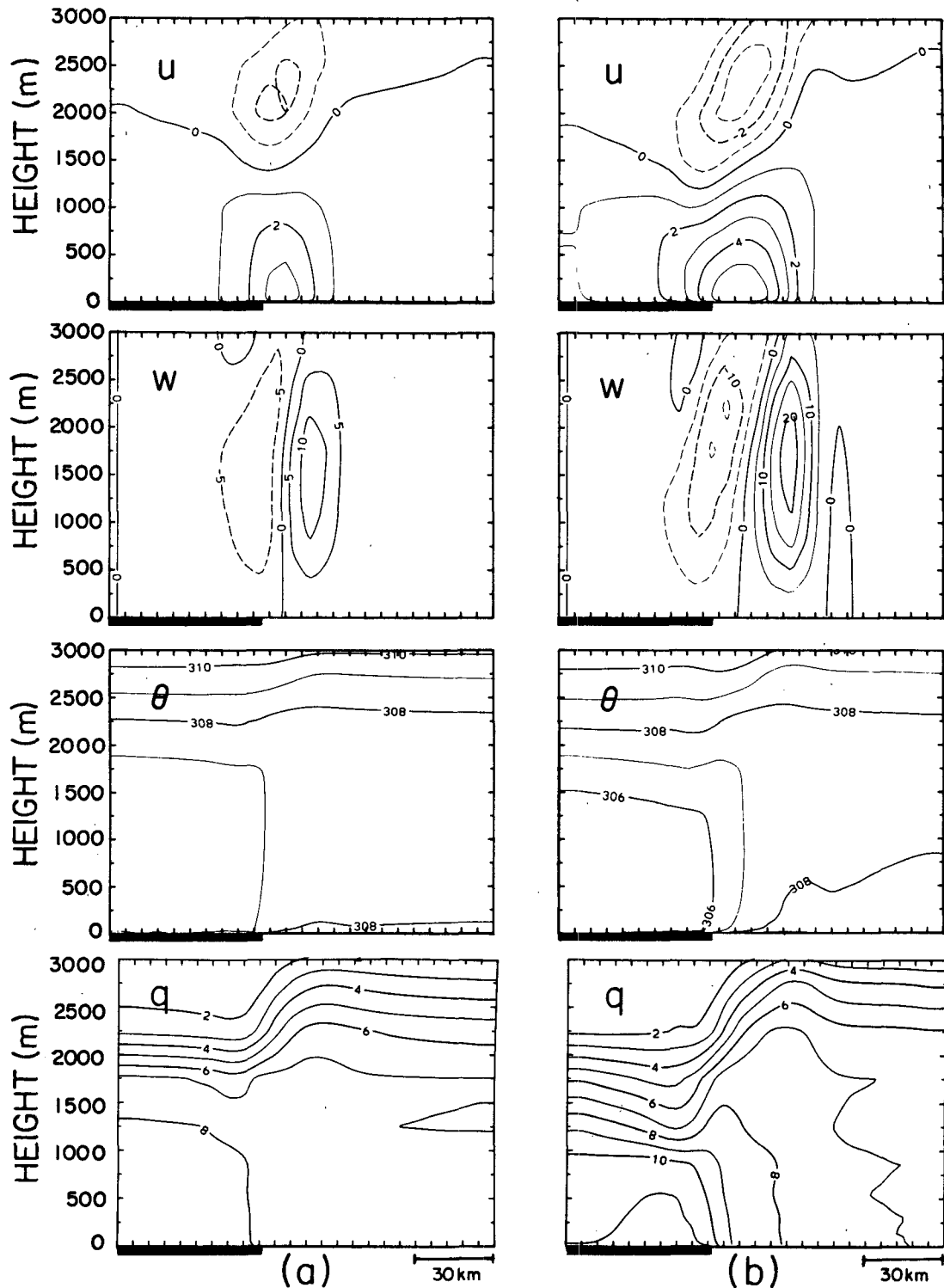


FIG. 6. Same as Fig. 5 except for a vegetation cover of 25% over the left-hand side of the domain simulated with (a) SSFP, and (b) BLP.

taken in Cache La Poudre Canyon, Colorado during the autumn of 1985. Whittaker (1956) and Whittaker and Niering (1965) documented large gradients of

vegetation types as a function of slope orientation (and altitudes) for the Great Smoky Mountains and the Santa Catalina Mountains (Arizona).

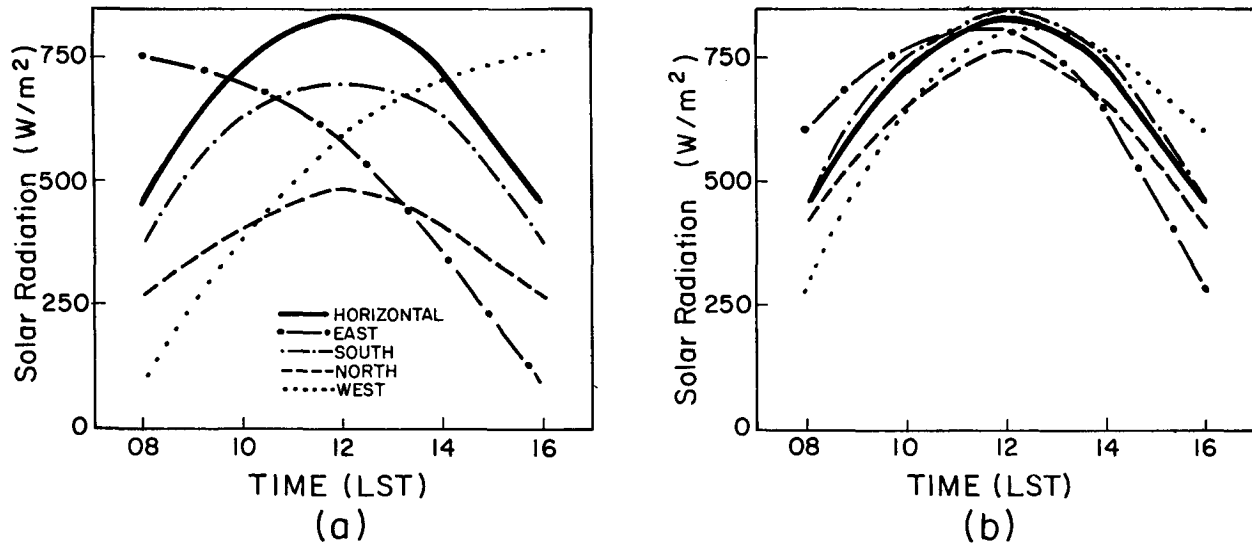


FIG. 7. The diurnal variation of solar global radiation received at the surface of a horizontal surface and on slopes facing north, east, south, and west, on 15 July at a latitude of 37°N. The slopes inclinations are (a) 45°, and (b) 15°.

In the following numerical experiments, a two-dimensional domain which consists of 10 grid intervals of 6 km width is considered. Two subgrid classes of randomly distributed “north-facing slopes” and “south-facing slopes” were defined, each one with a distribu-

tion of 50% within a grid cell. This domain was juxtaposed with 15 grid cells of flat terrain. The entire region was assumed to be bare and dry, and in the hilly part of the domain, subgrid-scale slopes of 45° (Figs. 9a and 10a) and 15° (Figs. 9b and 10b) were simulated.



FIG. 8. The contrast of natural vegetation obtained on a south-facing slope (left-hand side of the picture) and on a north-facing slope (right-hand side of the picture) in Cache La Poudre Canyon, Colorado, during the autumn of 1985.

The peak values of sensible heat fluxes simulated on the 45° south-facing and north-facing slopes are 370 and 180 W m<sup>-2</sup>, respectively, giving a global flux of 275 W m<sup>-2</sup> for the hilly region. The corresponding value for the flat region is 440 W m<sup>-2</sup>. This relatively large difference in sensible heat flux between the hilly and the flat regions of the simulation domain, which is directly related to the difference of solar radiation received at the ground surface (Fig. 7), generates a significant local circulation as illustrated in Fig. 10a. With the 15° sloping surfaces, however, only a minor variation of the sensible heat flux and the surface temperature is simulated for the different areas of the domain (Fig. 9b). For instance, less than 20 W m<sup>-2</sup> separates the global sensible heat flux of the hilly region from that of the flat region. As a result only a small perturbation of the meteorological fields occurs (Fig. 10b).

When these same slopes and the flat area are completely covered with dense vegetation ( $\sigma_f = 1.0$ , LAI = 3), the difference in sensible heat flux between the

hilly and flat areas, as well as its variation with the different slopes is very small, and only a very weak circulation is generated between the hilly and the flat regions, even for the 45° slopes, as illustrated in Fig. 11. Since the incoming solar radiation is weaker on the 45° north-facing slopes than on the 45° south-facing slopes and on the horizontal surfaces, the latent heat flux on the north-facing slopes is about 40% and 35% of that computed for the south-facing slopes and the flat area, respectively (Fig. 12). Plant water needs are consequently considerably lower on the north-facing slopes than on the other surfaces, explaining in part the sharp contrast of vegetation depicted in Fig. 8.

For the simulations presented in Figs. 13 and 14, the subgrid surface classes of the hilly region of the previous numerical experiments were redefined as “vegetated, 45° north-facing slopes” and “bare, dry, 45° south-facing slopes.” This hilly region was juxtaposed with a flat, bare, dry region (Figs. 13a and 14a) and with a flat, vegetated region (Figs. 13b and 14b).

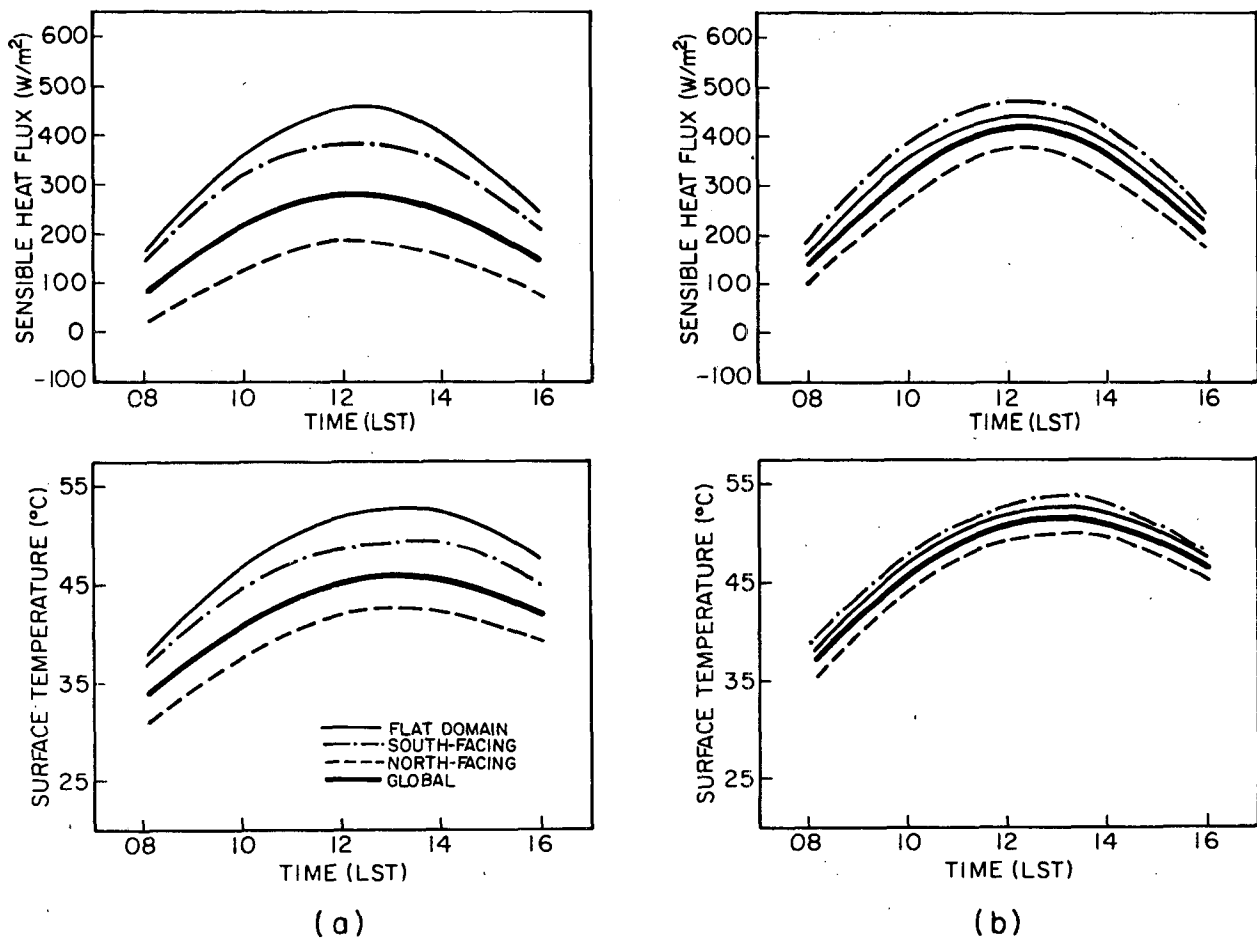


FIG. 9. The diurnal variation of sensible heat flux and surface temperature simulated for a horizontal dry surface and for dry north-facing and south-facing slopes. The inclinations of the slopes are (a) 45°, and (b) 15°.

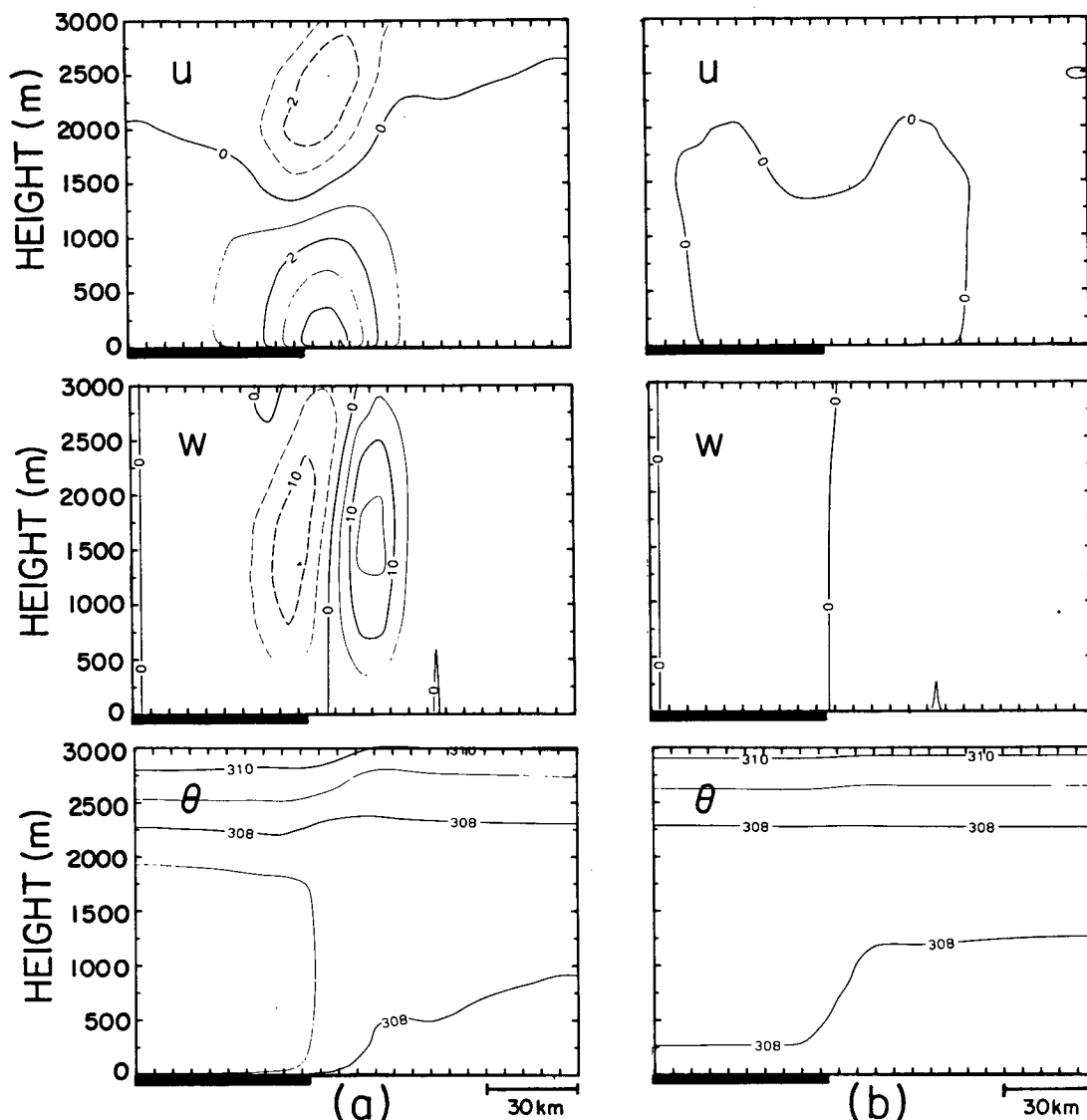


FIG. 10. Vertical cross section of the simulated region at 1400 LST for: (i) the horizontal wind component parallel to the domain ( $u$ ) in  $m\ s^{-1}$ , positive from left to right; (ii) the vertical wind component ( $w$ ) in  $cm\ s^{-1}$ , positive upward; and (iii) the potential temperature ( $\theta$ ) in K, resulting from the contrast of a 60-km-wide hilly region (indicated by the dark underbar) which consists of 50% north-facing and 50% south-facing subgrid-scale slopes, and a 90-km-wide dry flat region. The inclinations of the slopes are (a)  $45^\circ$ , and (b)  $15^\circ$ .

Considering each subgrid area individually, the heat fluxes and surface temperatures are only slightly different from the corresponding values in the “entirely bare” and “fully vegetated” cases depicted in Figs. 9a and 11. These differences are related to the interactions between the surface and the atmosphere explained in section 3a. The maximum global sensible heat flux in the hilly region is about  $200\ W\ m^{-2}$ . Juxtaposed with the sensible heat flux of the bare, dry, flat area (about  $400\ W\ m^{-2}$ ) it generates a relatively strong circulation (Fig. 14a). Juxtaposed, however, with the sensible heat flux obtained in the vegetated, flat area (about  $70\ W\ m^{-2}$ ) a much weaker circulation develops in the op-

posite direction, i.e., from the flat to the hilly region (Fig. 14b).

Since the diurnal distribution of solar radiation received on an east-facing slope and on a west-facing slope is very different, and also different from north-facing and south-facing slopes surfaces (Fig. 7), the fluxes and surface temperatures for terrain oriented in these directions are also expected to be different. This is demonstrated in Fig. 15, which illustrates the simulations of a hilly region consisting of 4 subgrid surface classes of equal distribution, each one corresponding to a cardinal compass orientation, juxtaposed with a flat area. The entire domain was assumed dry, and

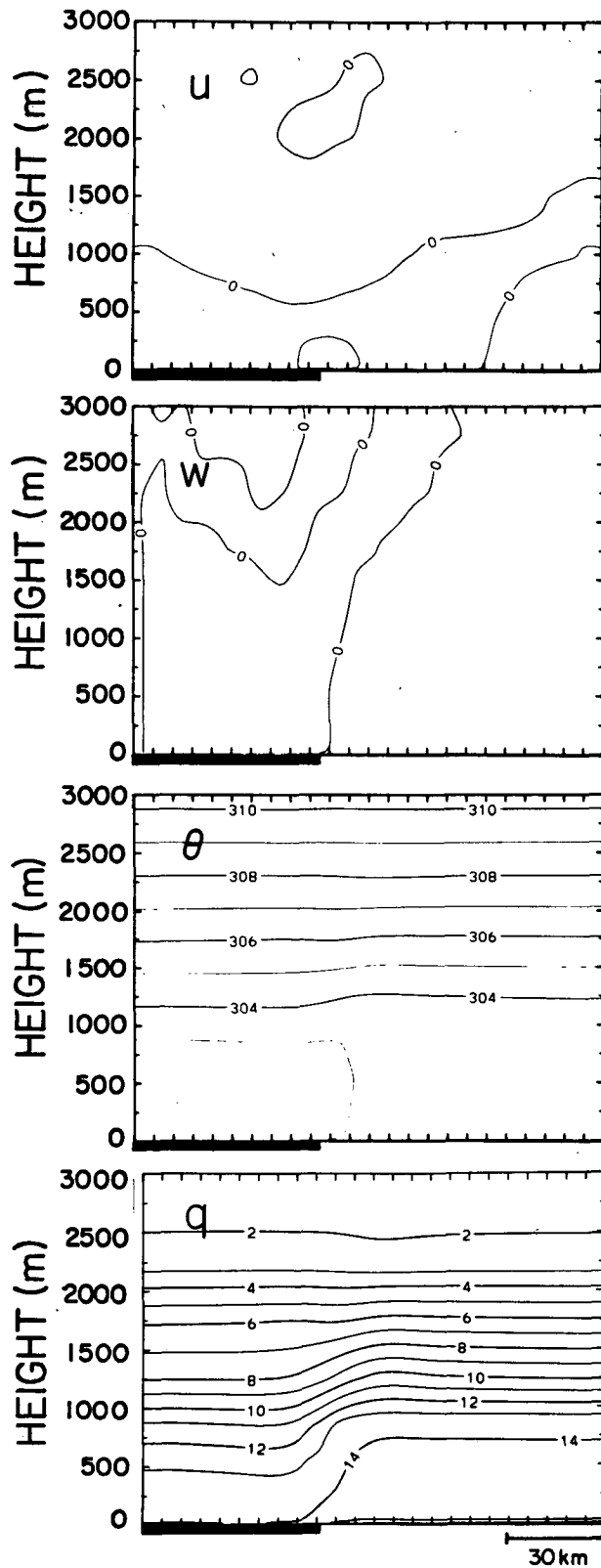


FIG. 11. Same as Fig. 10a except for a surface completely covered by dense unstressed vegetation. The specific humidity ( $q$ ) in  $\text{g kg}^{-1}$  is also represented.

slopes of  $45^\circ$  were considered. It is interesting to note that the global sensible heat flux in the hilly region is only slightly different from that obtained in the simulation of 50% north-facing and 50% south-facing slopes (Fig. 9). As a result, the local circulation generated by the juxtaposition of a hilly domain made up of these four slope classes and a flat region is almost identical to that generated by the juxtaposition of a hilly terrain with only north-facing and south-facing subgrid-scale surfaces and a flat region (Fig. 10a).

The few idealized cases described in this section have demonstrated the role which small topographical features may play on local meteorology when juxtaposed with flat areas. It is, however, not likely that such regular heterogeneities will be observed in the real world. As a matter of fact, the distribution of slope inclinations and orientations in a small region represented by a single grid cell in a meteorological model is generally much more complex. As illustrated by some of the examples presented here, however, the generated circulations do not seem to be very sensitive to small topographical variations, especially when the region is covered by unstressed vegetation. Therefore, a rough subgrid-scale topographical classification may be sufficient, at least in some cases, for the needs of meteorological studies. Additional experiments are required to derive general conclusions. The use of terrain spectra such as applied by Pielke and Kennedy (1980), and Young and Pielke (1983) may provide geometric information which will permit the more general representation of subgrid-scale terrain inhomogeneities.

### c. Land use heterogeneities

In addition to heterogeneities due to topographical features, land use diversity may also create very large surface heterogeneities in a small area. Typical classes of land use that can be found in rural and urban regions are asphalt, concrete and buildings, parks and other green areas, bodies of water, agricultural crops and orchards, forests, and wastelands. In order to simulate the surface forcing and the "regional micrometeorology" of such heterogeneous regions, four subgrid classes were defined in the model: (i) built-up areas and wastelands (20% of the total region), which are differentiated from bare-soil by initial homogeneous vertical soil values of temperature and humidity of 305 K and  $0.04 \text{ m}^3 \text{ m}^{-3}$ , respectively; (ii) bodies of water (10%) initialized with a surface temperature of 300 K; (iii) agricultural crops (40%); and (iv) forests (30%), which are differentiated from agricultural crops by a partial stomatal aperture.

In the numerical experiments presented in Figs. 16 and 17, ten grid cells of heterogeneous land (each 6 km wide) were juxtaposed with (i) 15 uniformly dry and bare grid cells (Figs. 16a and 17a), and (ii) 15 homogeneously vegetated grid cells (Figs. 16b and 17b). This land distribution was selected arbitrarily

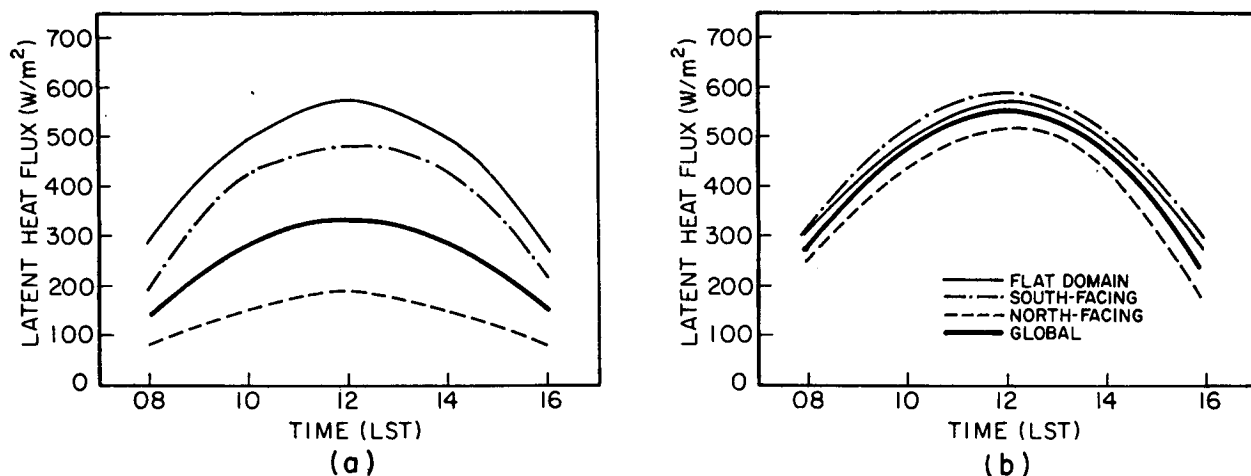


FIG. 12. The diurnal variation of latent heat flux on a horizontal surface and north-facing and south-facing slopes completely covered by dense unstressed vegetation. The inclinations of the slopes are (a) 45°, and (b) 15°.

but is quite representative of rural and small urban regions. The juxtaposition with the vegetated area may correspond to the early summer season when natural vegetation is well developed. The juxtaposition with the dry, bare land may correspond to the end of the summer season after the natural vegetation has perished.

In the heterogeneous region, the fluxes and surface temperatures are very different for each subgrid class. The range of maximum sensible heat flux is between  $-10 \text{ W m}^{-2}$  (for bodies of water) to  $450 \text{ W m}^{-2}$  (for built-up areas), that of latent heat flux is between  $0 \text{ W m}^{-2}$  (for built-up areas) to  $610 \text{ W m}^{-2}$  (for agricultural crops), and the range of surface temperature is between  $27^\circ\text{C}$  (for bodies of water) to  $50^\circ\text{C}$  (for built-up areas). The grid-cell global fluxes are related to the distribution of the subgrid classes, and, therefore, in the present examples they are more influenced by vegetation (forest and agricultural areas constitute 70% of the heterogeneous grid cells) than by built-up areas and bodies of water. As a result, the global sensible heat flux from the heterogeneous grid cells is relatively small, with a peak value of about  $155 \text{ W m}^{-2}$ . The contrast between a bare, dry, homogeneous region and the heterogeneous region generates a strong circulation (Fig. 17a). The contrast, however, with a vegetated region for which the peak value of the sensible heat flux is only about  $70 \text{ W m}^{-2}$ , results in a relatively weak circulation that develops in the opposite direction (Fig. 17b).

The two-dimensional simulations described in this section were initialized with calm atmospheric conditions ( $u = 0.5 \text{ m s}^{-1}$ ) in order to emphasize the local circulations which may develop as a result of extensive contrasts of sensible heat flux. When the initial background wind in the atmosphere is stronger, however, the rapid inland movement of relatively cold air reduces the pressure gradients between the adjacent areas and,

consequently, the circulation. This process is demonstrated in Fig. 18 by simulating the heterogeneous land described in the previous numerical experiment (20% built-up areas and wastelands, 10% bodies of water, 40% agricultural crops, and 30% forests) juxtaposed with a bare, dry land and initializing the atmospheric flow with a moderate geostrophic wind of  $5 \text{ m s}^{-1}$  from the heterogeneous land to the bare, dry land. The stronger wind at the surface increases the sensible heat fluxes from the subgrid areas by a factor of about 20%, the latent heat fluxes by a factor of about 10%, and cools the surface temperatures by a few degrees Kelvin. Although the gradient of sensible heat flux between the heterogeneous and the homogeneous areas increased from a peak value of  $245 \text{ W m}^{-2}$  for the calm atmosphere to a peak value of  $325 \text{ W m}^{-2}$  in the windy case, the atmosphere is much less disturbed under windy conditions, as illustrated by the variation of wind, temperature, and humidity in Fig. 18. As discussed by Mahrer and Pielke (1978), synoptic winds which advect cool near-surface air towards a warmer land surface will result in a weaker mesoscale circulation as a result of the spreading of the horizontal mesoscale pressure gradient force. In contrast, a synoptic wind of  $5 \text{ m s}^{-1}$  from the warmer land towards the cooler surface will tighten the mesoscale horizontal pressure gradient force and result in a stronger mesoscale circulation (Estoque 1961).

It is interesting to note that the diurnal surface temperature of strongly transpiring surfaces (e.g., agricultural crops) fluctuates when the atmosphere is initially calm (Fig. 16). This is mainly related to the gradient of specific humidity in the surface layer. During the late afternoon, and occasionally during the early morning, the gradient of specific humidity is typically zero or even negative. As a result, the latent heat flux falls to zero and the surface temperature is relatively

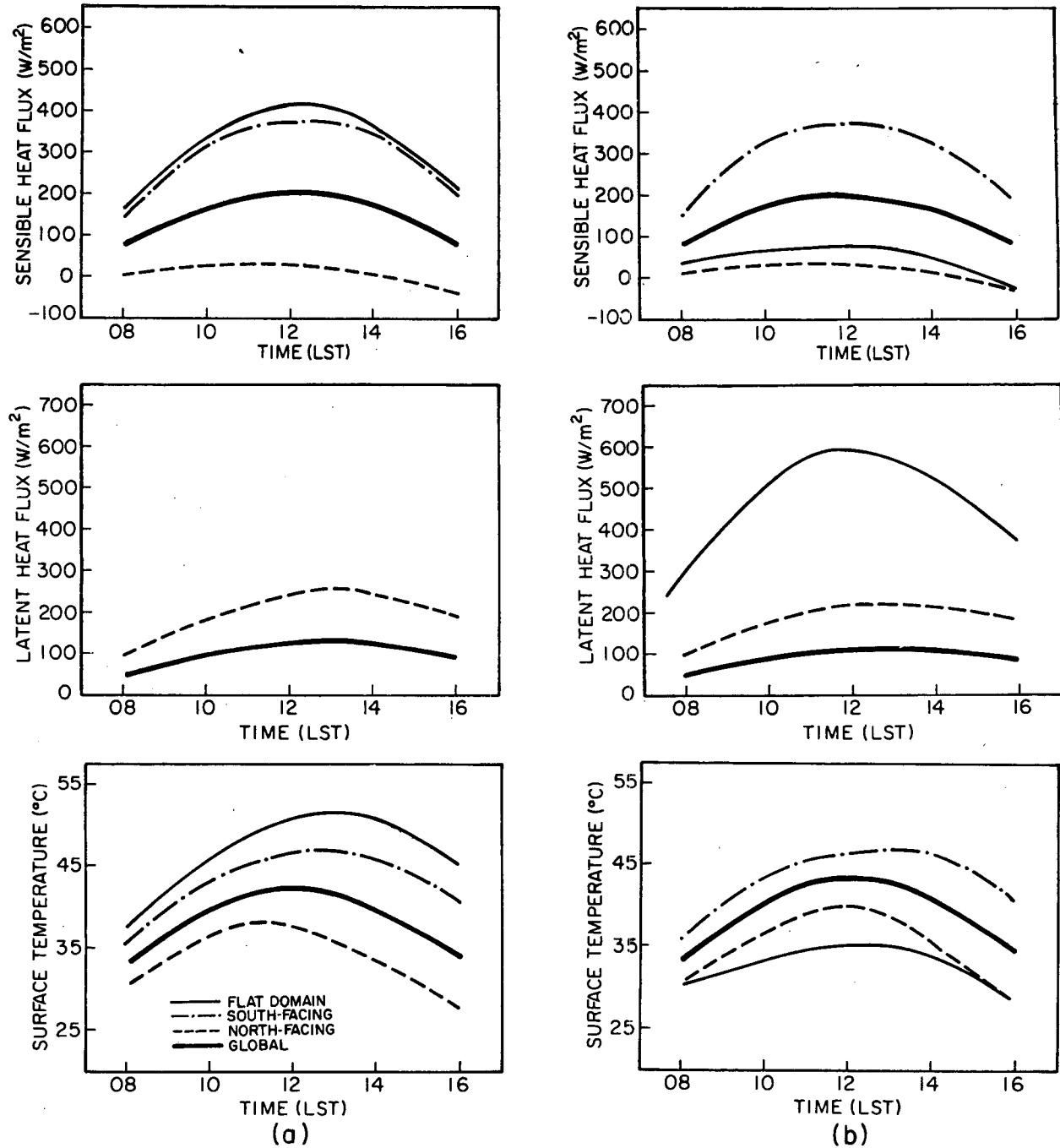


FIG. 13. The simulated diurnal variation of sensible heat flux, latent heat flux and surface temperature for a horizontal surface, a  $45^{\circ}$  north-facing slope completely covered by unstressed vegetation, and a bare, dry,  $45^{\circ}$  south-facing slope. The horizontal surface is (a) bare and dry, and (b) completely covered by unstressed vegetation.

high. During most of the day, however, the crops transpire well and the surface layer is less humid than in the evening. Therefore, a large latent heat flux is possible and a relatively low vegetation temperature is ob-

tained. This phenomenon is not observed with strong winds because of the better mixing of the humidity in the atmosphere and its advection away from the transpiring zones.

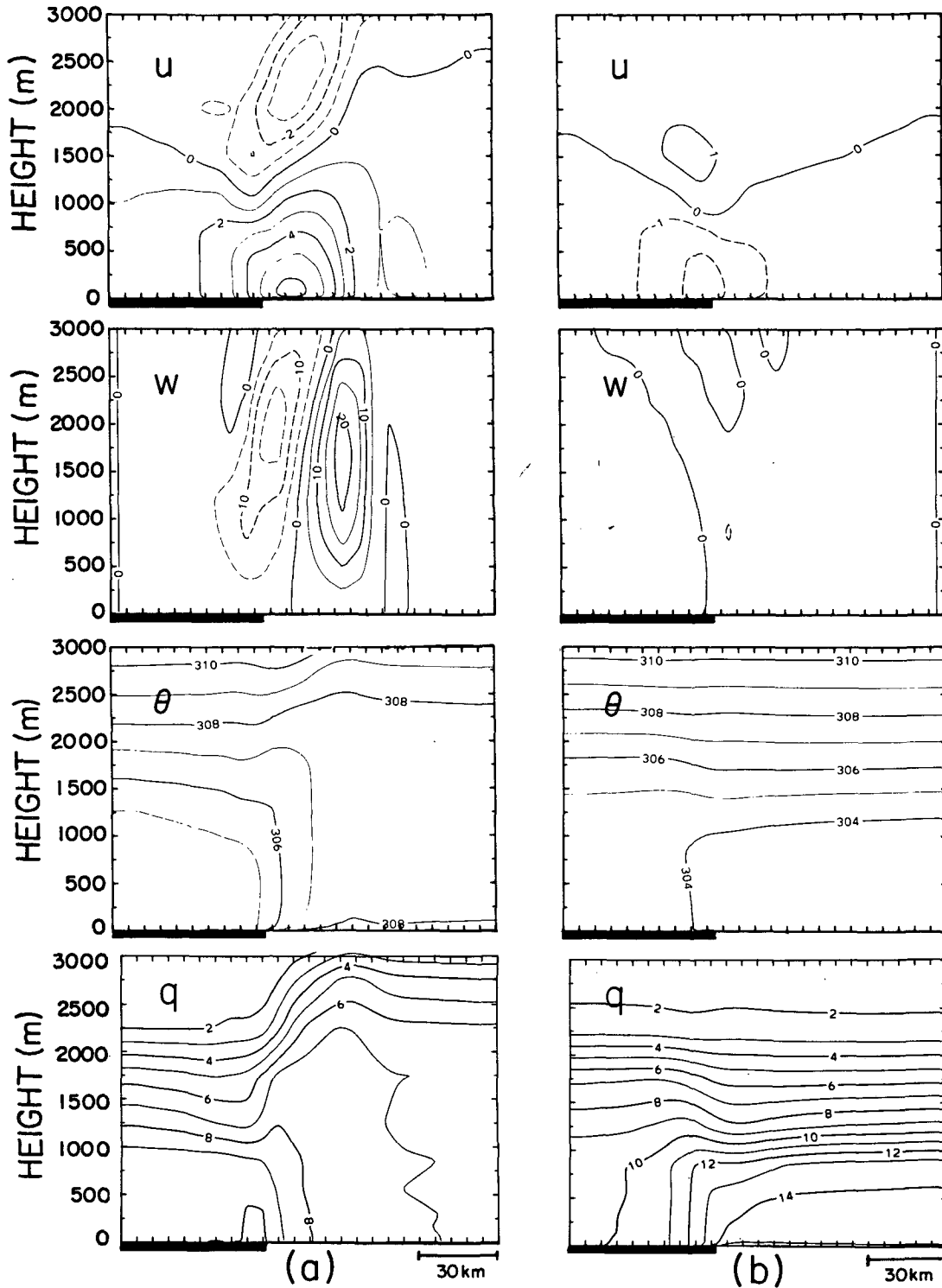


FIG. 14. Vertical cross section of the simulated region at 1400 LST for: (i) the horizontal wind component parallel to the domain ( $u$ ) in  $m s^{-1}$ , positive from left to right; (ii) the vertical wind component ( $w$ ) in  $cm s^{-1}$ , positive upward; (iii) the potential temperature ( $\theta$ ) in K; and (iv) the specific humidity ( $q$ ) in  $g kg^{-1}$ , resulting from the contrast of a 60-km-wide, hilly region (indicated by the dark underbar) which consists of 50% subgrid-scale,  $45^\circ$  north-facing slopes completely covered by unstressed vegetation and 50% bare, dry,  $45^\circ$  south-facing slopes, and a 90-km-wide horizontal region. The horizontal region is (a) bare and dry, and (b) completely covered by unstressed vegetation.

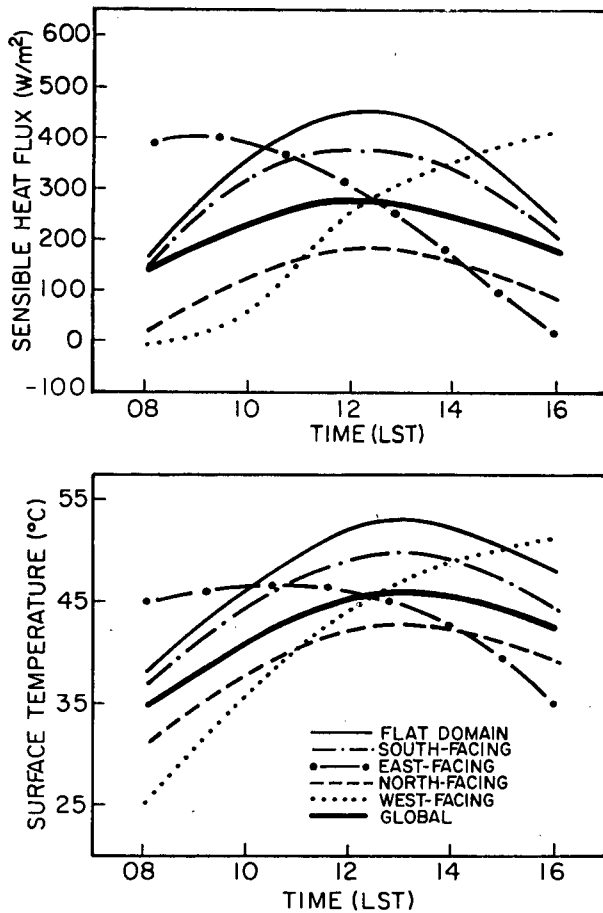


FIG. 15. Same as Fig. 9a except bare, dry slopes facing east and west are also represented.

#### 4. Summary and conclusions

Because of the diversity of land use and the variation of topography found in even a small area, atmospheric numerical models which assume homogeneous land characteristics may fail to represent properly the forcing at the ground surface. In the present study, a parameterization for subgrid-scale heterogeneous surfaces (SSFP) was suggested and its impact on mesoscale circulations and on regional micrometeorology was evaluated for a few typical cases. This new parameterization makes possible the simulation of any land surface without significantly increasing the computer resources required to run the model. It is based on the assumption that horizontal fluxes between the different land patches in a single grid cell of the numerical model are small as compared to the vertical fluxes. Therefore, small circulations which may develop in practice between the land patches are assumed insignificant as compared to the main flow over the terrain. This assumption will need to be validated. However, previous studies (e.g., Pielke 1984) suggest that background circulations in-

hibit the development of local smaller-scale organized circulations.

The formulation of Businger et al. (1971) used in our model parameterization was developed based on field experiments in a homogeneous, flat domain. Thus, when the grid cell is very heterogeneous and the size of each homogeneous patch is small, this formulation might not be appropriate and should be used with reservation. Additional field experimentation is required to assess and extend the validity of surface similarity theory to small-scale surface inhomogeneities.

A simple heterogeneous case (partial vegetation cover) was simulated with a bulk layer parameterization (BLP) and SSFP in order to demonstrate the benefits of the new parameterization. Even though it seems possible to simulate mesoscale atmospheric patterns with either of the two parameterizations for several of the simple cases considered in this paper, SSFP also provides detailed micrometeorological conditions of the different land patches within the region simulated by the model. Avissar and Mahrer (1988b) have already discussed the shortcomings of the "grid representative micrometeorological conditions" in their attempt to compare simulated nighttime minimum temperatures of an agricultural heterogeneous area with observations carried out at particular locations in the region. Operational decisions in modern agriculture related to various applications such as irrigation, fertilization, phytopathological treatments, and so forth are usually partially based on plant environmental conditions such as temperature, humidity, and wind speed. In this study, it was demonstrated that large discrepancies can be obtained between the micrometeorological conditions simulated by BLP and SSFP, and that a mesoscale numerical model coupled with SSFP offers improved capabilities for agricultural research and management. Applications of the model to other research disciplines with similar needs such as ecology and hydrology can also be considered. The simulation of hilly regions presented in section 3b, for example, can be elaborated to achieve a better understanding of the preference of a particular plant to grow at particular locations. Problems involved in the use of satellite measurements to infer surface energy budget and evapotranspiration have been extensively discussed in the literature (e.g., Wetzel and Chang 1988). Provided that appropriate land use information is available, the model may also be helpful at this task.

In the simulations presented in this study, soil wetness in the root zone as well as environmental conditions were always assumed optimal for plant transpiration. Stress conditions (e.g., warm ambient air, lack of water in the soil, etc.) tend to lead to various degrees of stomatal closure. Thus a reduction in the transpiration rates and a rise of the sensible heat flux is expected. Obviously, for such situations, the contrast of sensible heat flux between a vegetated area and an adjacent dry

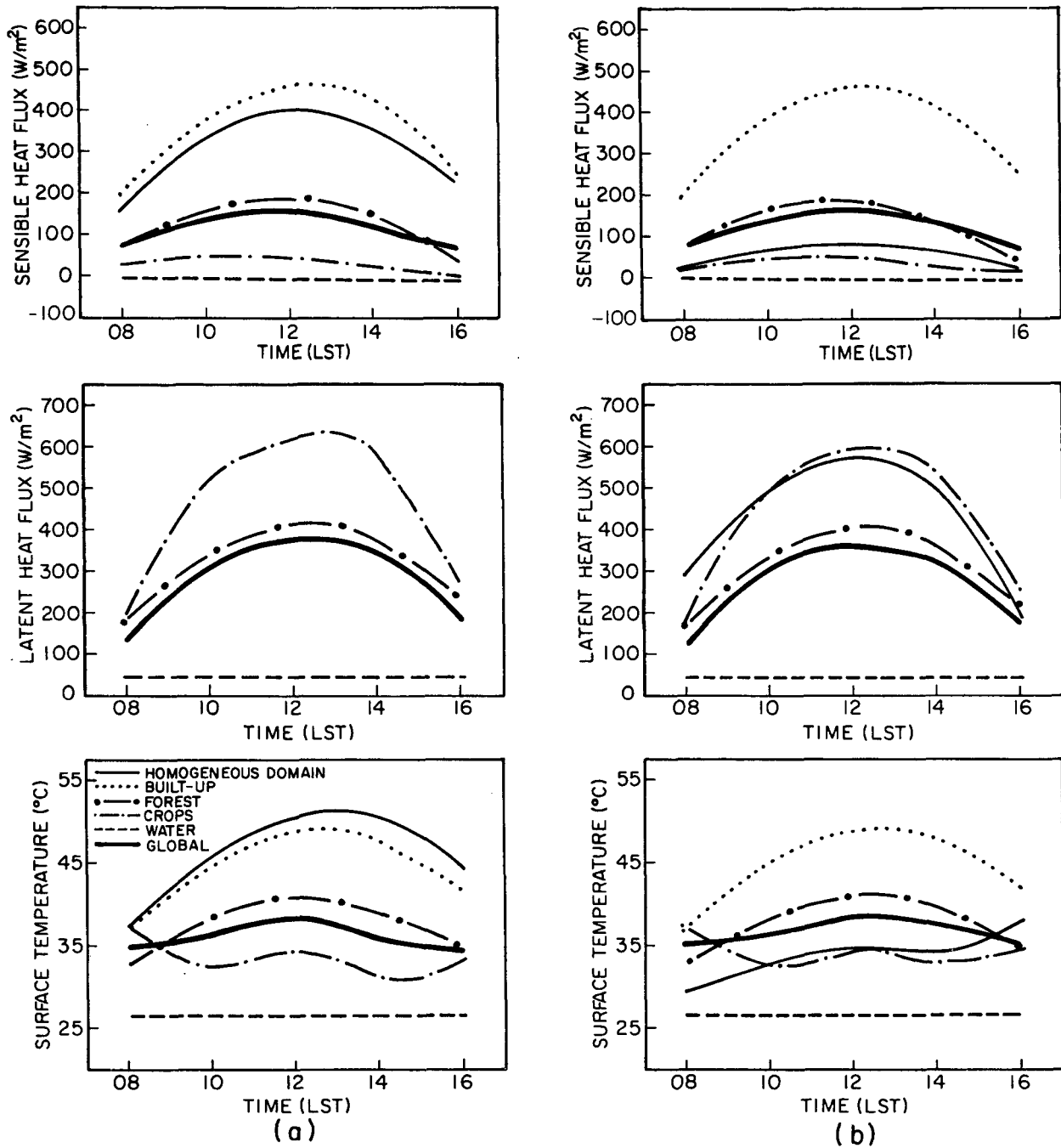


FIG. 16. The diurnal variation of sensible heat flux, latent heat flux and surface temperature simulated for a heterogeneous land surface which consists of 20% built-up areas and wastelands, 10% bodies of water, 40% agricultural crops, and 30% forests. The heterogeneous region is juxtaposed with (a) bare, dry land, and (b) land completely covered by unstressed vegetation.

region decreases, and consequently reduces the intensity of the generated circulations.

As discussed in the present study as well as in previous ones (e.g., Ookouchi et al. 1984; Mahfouf et al. 1987; Segal et al. 1988), the magnitude of the local

circulations is related to the horizontal gradient of sensible heat flux and the background atmospheric forcing. A systematic analysis of these processes is, however, still required to improve our understanding of such circulations.

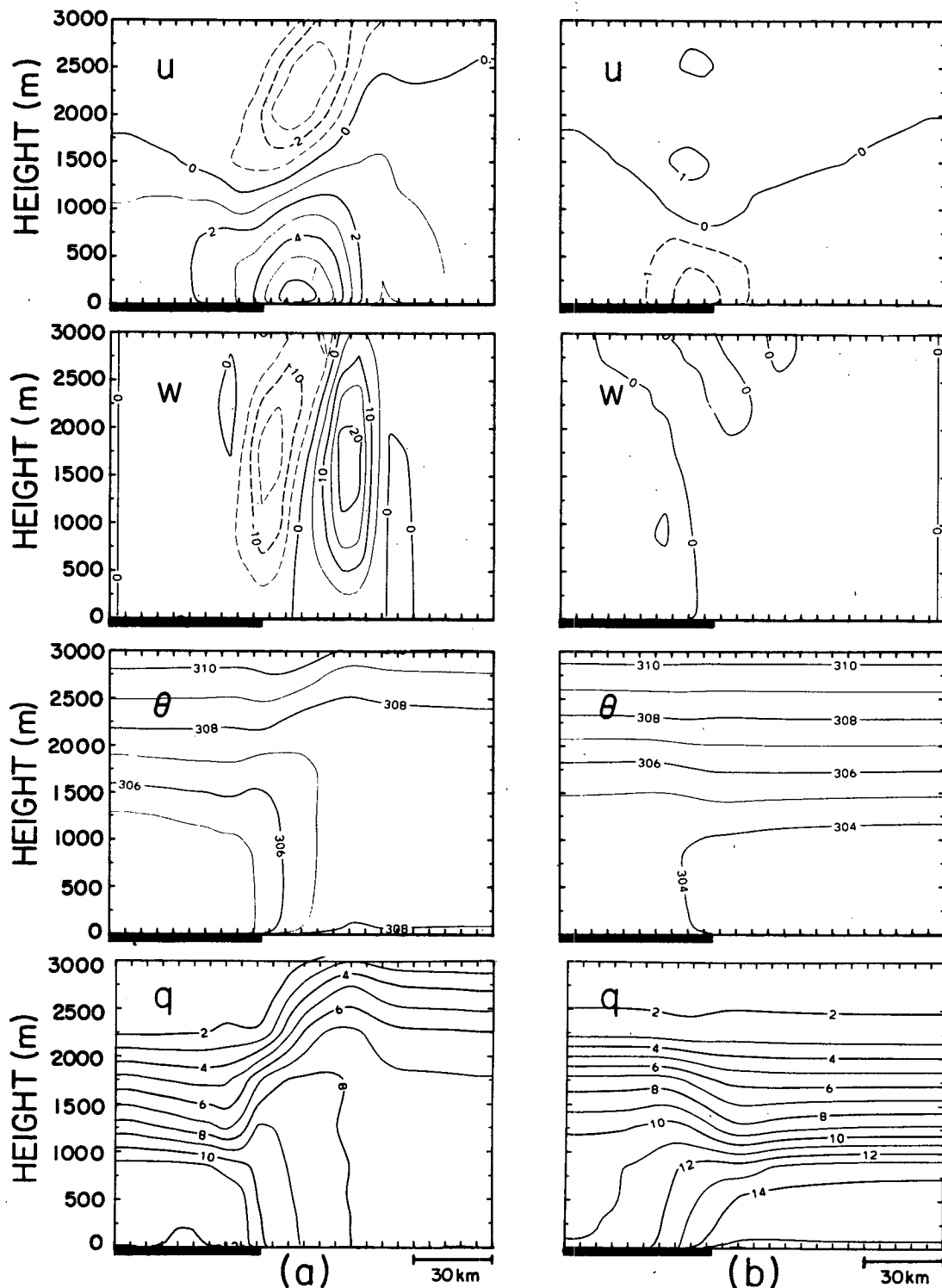


FIG. 17. Same as Fig. 14 except the dark underbar indicates a heterogeneous land surface which consists of 20% built-up areas and wastelands, 10% bodies of water, 40% agricultural crops, and 30% forests.

Finally, the definition of subgrid class types and area is a critical process for the initialization of the model. In regard to atmospheric impact, a particular class

might or might not be of significance for a particular simulation, according to its contribution to the grid-scale global sensible heat flux (which is a function of

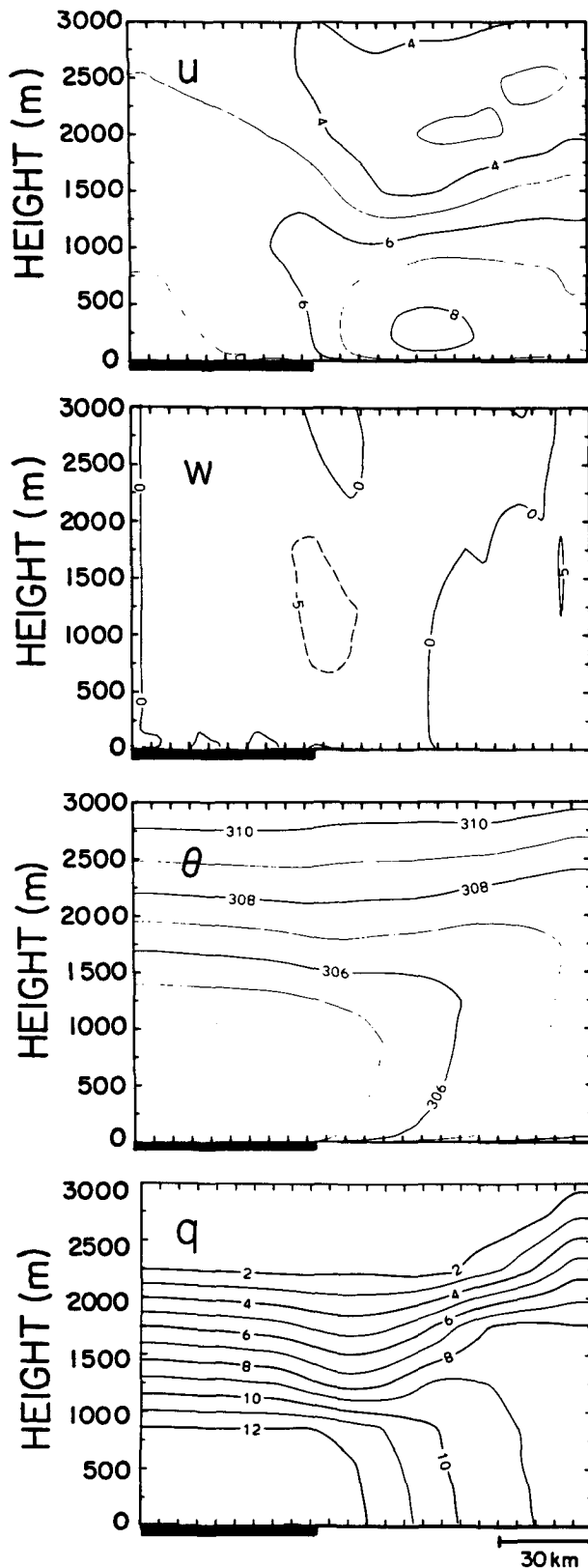


FIG. 18. Same as Fig. 17a except initialized with a moderate background wind of  $5 \text{ m s}^{-1}$  parallel to the domain ( $u$  positive).

its area and its water availability for evapotranspiration) and the global environment of the region considered in the simulation. An extensive sensitivity analysis should be dedicated to this study and is planned in the near future.

*Acknowledgments.* This research was supported by the National Science Foundation under Grant ATM-8616662 and by Office of Naval Research Grant N00014-88-K-0029. Computations were performed using the National Center for Atmospheric Research CRAY computer (NCAR is supported by NSF). The authors wish to thank Michael Moran and an anonymous reviewer for their meticulous review of the manuscript and for making important suggestions. Peter Wetzel, Isaac Mahrer, and Ofir Naot are also thanked for making valuable comments. The manuscript was professionally prepared by Bryan Critchfield and Dallas McDonald, and the drafting was prepared by Judy Sorbie.

#### REFERENCES

- Abbs, D. J., and R. A. Pielke, 1986: Thermally forced surface flow and convergence patterns over northeast Colorado. *Mon. Wea. Rev.*, **114**, 2281–2296.
- Avissar, R., and Y. Mahrer, 1982: Verification study of a numerical greenhouse microclimate model. *Trans. Amer. Soc. Agric. Eng.*, **25**(6), 1711–1720.
- , and —, 1986: Water desalination in solar earth stills: A numerical study. *Water Resour. Res.*, **22**, 1067–1075.
- , and —, 1987: A pseudo three-dimensional numerical model of the soil-plant-atmosphere system. *Agriculture Forest Meteorology Conference*, W. Lafayette, Indiana, 60–62.
- , and —, 1988a: Mapping frost-sensitive areas with a three-dimensional local scale model. Part I: Physical and numerical aspects. *J. Appl. Meteor.*, **27**, 400–413.
- , and —, 1988b: Mapping frost-sensitive areas with a three-dimensional local scale model. Part II: Comparison with observations. *J. Appl. Meteor.*, **27**, 414–426.
- , N. Dagan and Y. Mahrer, 1986: Evaluation, in real-time, of the actual evapotranspiration using a numerical model. *Agrotique 86, Automation and Robots for Agriculture*. Bordeaux, France, 255–263 (available from the authors).
- , P. Avissar, Y. Mahrer and B. A. Bravdo, 1985: A model to simulate response of plant stomata to environmental conditions. *Agric. For. Meteorol.*, **34**, 21–29.
- , M. Segal, J. Weaver and R. A. Pielke, 1987: Thermally induced circulations resulting from non-uniform surface characteristics across meso- $\beta$  domains: Satellite and model evaluations. *IA-MAP/IUGG Conference*, Vancouver, (Abstracts).
- Businger, J. A., J. C. Wyngaard, Y. Izumi and E. F. Bradley, 1971: Flux-profile relationships in the atmospheric surface layer. *J. Atmos. Sci.*, **28**, 181–189.
- Clapp, R., and G. Hornberger, 1978: Empirical equations for some soil hydraulic properties. *Water Resour. Res.*, **14**, 601–604.
- Clarke, R. H., 1970: Recommended methods for the treatment of the boundary layer in numerical models. *Aust. Meteor. Mag.*, **18**, 51–73.
- Deardorff, J. W., 1978: Efficient prediction of ground surface temperature and moisture, with inclusion of a layer of vegetation. *J. Geophys. Res.*, **83**, 1889–1903.
- De Vries, D. A., 1963: Thermal properties of soils. *Physics of Plant Environment*, Van Wijk, W. R., Ed., North Holland, Amsterdam, 210–235.
- Estoque, M. A., 1961: A theoretical investigation of the sea breeze. *Quart. J. Roy. Meteor. Soc.*, **87**, 136–146.

- Garrett, A. J., 1982: A parameter study of interactions between convective clouds, the convective boundary layer, and forested surface. *Mon. Wea. Rev.*, **110**, 1041-1059.
- Hanna, S. R., and S. D. Swisher, 1971: Meteorological effects of the heat and moisture produced by man. *Nucl. Saf.*, **12**, 114-122.
- , and F. A. Gifford, 1975: Meteorological effects of energy dissipation at large power parks. *Bull. Amer. Meteor. Soc.*, **56**, 1069-1077.
- Hills, R. C., and S. G. Reynolds, 1969: Illustrations of soil moisture variability areas and plots of different sizes. *J. Hydrol.*, **8**, 27-47.
- McCumber, M. C., and R. A. Pielke, 1981: Simulation of the effects of surface fluxes of heat and moisture in a mesoscale numerical model. *J. Geophys. Res.*, **86**, 9929-9938.
- McNider, R. T., and R. A. Pielke, 1981: Diurnal boundary-layer development over sloping terrain. *J. Atmos. Sci.*, **38**, 2198-2212.
- Mahfouf, J.-F., E. Richard and P. Mascart, 1987: The influence of soil and vegetation on the development of mesoscale circulations. *J. Climate Appl. Meteor.*, **26**, 1483-1495.
- Mahrer, Y., and R. A. Pielke, 1977: A numerical study of the air flow over irregular terrain. *Contrib. Atmos. Phys.*, **50**, 98-113.
- , and —, 1978: A test of an upstream spline interpolation technique for the advective terms in a numerical mesoscale model. *Mon. Wea. Rev.*, **106**, 818-830.
- , and R. Avissar, 1985: A numerical study of the effects of soil surface shape upon the temperature and moisture profiles. *Soil Sci.*, **139**, 483-490.
- Ookouchi, Y., M. Segal, R. C. Kessler and R. A. Pielke, 1984: Evaluation of soil moisture effects on generation and modification of mesoscale circulations. *Mon. Wea. Rev.*, **11**, 2281-2292.
- Philip, J. R., and D. A. De Vries, 1957: Moisture movement in porous materials under temperature gradients. *Trans. Amer. Geophys. Union*, **38**, 222-232.
- Pielke, R. A., 1974: A three-dimensional numerical model of the sea breezes over south Florida. *Mon. Wea. Rev.*, **102**, 115-139.
- , 1984: *Mesoscale Meteorological Modeling*. Academic Press, 612 pp.
- , and Y. Mahrer, 1975: Technique to represent the heated-planetary boundary layer in mesoscale models with coarse vertical resolution. *J. Atmos. Sci.*, **32**, 2288-2308.
- , and —, 1978: Verification analysis of the University of Virginia three-dimensional mesoscale model prediction over south Florida for 1 July 1973. *Mon. Wea. Rev.*, **106**, 1568-1589.
- , and E. Kennedy, 1980: Mesoscale Terrain Features. Rep. No. UVA-ENV SCI-MESO-1980-1 (available from R. A. Pielke, Dept. of Atmos. Sci., Colorado State University, Ft. Collins, CO 80523).
- Segal, M., Y. Mahrer and R. A. Pielke, 1982: Application of a numerical mesoscale model for the evaluation of seasonal persistent regional climatological patterns. *J. Appl. Meteor.*, **21**, 1754-1762.
- , R. Avissar, M. C. McCumber and R. A. Pielke, 1988: Evaluation of vegetation effects on the generation and modification of mesoscale circulations. *J. Atmos. Sci.*, **45**, 2268-2292.
- Sellers, P. J., Y. Mintz, Y. C. Sud and A. Dalcher, 1986: A simple biosphere model (SiB) for use within general circulation models. *J. Atmos. Sci.*, **43**, 505-531.
- Sharon, D., 1980: The distribution of hydrologically effective rainfall incident on sloping ground. *J. Hydrol.*, **46**, 165-188.
- Shaw, R. H., and W. L. Decker, 1977: The general heat balance of canopies. *Modification of the Aerial Environment of Plants*, B. J. Barfield and J. F. Gerber, Eds., American Society of Agricultural Engineers, 141-155.
- Wetzel, P. J., and J.-T. Chang, 1988: Evapotranspiration from non-uniform surfaces: A first approach for short-term numerical weather prediction. *Mon. Wea. Rev.*, **116**, 600-621.
- Whittaker, R. H., 1956: Vegetation of the Great Smoky Mountains. *Ecological Monographs*, **26**, 1-80.
- , and W. A. Niering, 1965: Vegetation of the Santa Catalina Mountains, Arizona: A gradient analysis of the south slope. *Ecology*, **46**, 429-452.
- Wilson, M. F., A. Henderson-Sellers, R. E. Dickinson and P. J. Kennedy, 1987: Sensitivity of the Biosphere-Atmosphere Transfer Scheme (BATS) to the inclusion of variable soil characteristics. *J. Climate Appl. Meteor.*, **26**, 341-362.
- Young, G., and R. A. Pielke, 1983: Application of terrain height variance spectra to mesoscale modeling. *J. Atmos. Sci.*, **40**, 2555-2560.
- Zhang, D., and R. A. Anthes, 1982: A high-resolution model of the planetary boundary layer-sensitivity tests and comparisons with SESAME-79 data. *J. Appl. Meteor.*, **21**, 1594-1609.